Variation in Global Chemical Composition of PM$_{2.5}$: Emerging Results from SPARTAN

Graydon Snider[1], Crystal L. Weagle[2], Kalaivani K. Murdymootoo[1], Amanda Ring[1], Yvonne Ritchie[1], Emily Stone[1], Ainsley Walsh[1], Clement Akoshile[3], Nguyen Xuan Anh[4], Rajasekhar Balasubramanian[5], Jeff Brook[6], Fatimah D. Qonitan[7], Jinlu Dong[8], Derek Griffith[9], Kebin He[8], Brent N. Holben[10], Ralph Kahn[10], Nofel Lagrosas[11], Puji Lestari[7], Zongwei Ma[12], Amit Misra[13], Leslie K. Norford[14], Eduardo J. Quel[15], Abdus Salam[16], Bret Schichtel[17], Lior Segev[18], S.N. Tripathi[13], Chien Wang[19], Chao Yu[20], Qiang Zhang[8], Yuxuan Zhang[8], Michael Brauer[21], Aaron Cohen[22], Mark D. Gibson[23], Yang Liu[18], J. Vanderlei Martins[24], Yinon Rudich[18], Randall V. Martin*[1,2,25]

*Corresponding author email: graydon.snider@dal.ca or randall.martin@dal.ca phone: 902-494-1820, fax: 902-494-5191

Affiliations
[1]Department of Physics and Atmospheric Science, Dalhousie University, Halifax, Canada
[2]Department of Chemistry, Dalhousie University, Halifax, Canada
[3]Department of Physics, University of Ilorin, Ilorin, Nigeria
[4]Institute of Geophysics, Vietnam Academy of Science and Technology, Hanoi, Vietnam
[5]Department of Civil and Environmental Engineering, National University of Singapore
[6]Department of Public Health Sciences, University of Toronto, Toronto, Ontario, Canada M5S 1A8
[7] Faculty of Civil and Environmental Engineering, ITB, JL. Ganesha No.10, Bandung 40132, Indonesia
[8]Center for Earth System Science, Tsinghua University, Beijing, China
[9]Council for Scientific and Industrial Research (CSIR), Pretoria, South Africa
[10]Earth Science Division, NASA Goddard Space Flight Center, Greenbelt, Maryland, USA
[11]Manila Observatory, Ateneo de Manila University campus, Quezon City, Philippines
[12] School of Environment, Nanjing University, Nanjing, China.
[13] Center for Environmental Science and Engineering, Indian Institute of Technology Kanpur, India
[14] Department of Architecture, Massachusetts Institute of Technology, Cambridge, MA, 02139, USA
[15]UNIDEF (CITEDEF-CONICET) Juan B. de la Salle 4397 – B1603ALO Villa Martelli, Buenos Aires, Argentina
[16]Department of Chemistry, University of Dhaka, Dhaka - 1000, Bangladesh
[17] Cooperative Institute for Research in the Atmosphere, Colorado State, Colorado, USA
[18] Department of Earth and Planetary Sciences, Weizmann Institute, Rehovot 76100, Israel
[19]Center for Global Change Science, Massachusetts Institute of Technology, Cambridge, MA, 02139, USA
[20]Rollins School of Public Health, Emory University, 1518 Clifton Road NE, Atlanta, GA 30322, United States
[21]School of Population and Public Health, University of British Columbia, Vancouver, British Columbia, Canada
[22]Health Effects Institute, 101 Federal Street Suite 500, Boston, MA 02110-1817, USA
[23]Department of Process Engineering and Applied Science, Dalhousie University, Halifax, Canada,
[24]Department of Physics and Joint Center for Earth Systems Technology, University of Maryland, Baltimore County, Baltimore, Maryland, USA
[25]Harvard-Smithsonian Center for Astrophysics, Cambridge, MA 02138, USA

Abstract

The Surface PARTiculate mAtter Network (SPARTAN) is a long-term project that includes characterization of chemical and physical attributes of aerosols from filter samples collected worldwide. This manuscript discusses the ongoing efforts of SPARTAN to define and quantify major ions and trace metals found in fine particulate matter (PM$_{2.5}$). Our methods infer the spatial and temporal variability of PM$_{2.5}$ in a cost-effective manner. Gravimetrically-weighed filters represent multi-day averages of PM$_{2.5}$, with a collocated nephelometer sampling air continuously. SPARTAN instruments are paired with AErosol RObotic NETwork (AERONET) sun photometers to better understand the relationship between ground-level PM$_{2.5}$ and columnar aerosol optical depth (AOD).

We have examined the chemical composition of PM$_{2.5}$ at 12 globally dispersed, densely populated urban locations and a site at Mammoth Cave (US) National Park used as a background comparison. Each SPARTAN location has so far been active between the years 2013 and 2016 over 2 to 26 month periods, with an average period of 12 months per site. These sites have collectively gathered over 10 site-years of quality aerosol data. The major PM$_{2.5}$ constituents across all sites (relative contribution ± SD) are ammoniated sulfate (20% ± 11%), crustal material (13.4% ± 9.9%), equivalent black carbon (11.9% ± 8.4%), ammonium nitrate (4.7% ± 3.0%), sea salt (2.3% ± 1.6%), trace element oxides (1.0% ± 1.1%), water (7.2% ± 3.3%) at 35% RH, and residual matter (40% ± 24%).

Analysis of filter samples reveals that several PM$_{2.5}$ chemical components varied by more than an order of magnitude between sites. Ammoniated sulfate ranges from 1.1 μg m^{-3} (Buenos Aires, Argentina) to 17 μg m^{-3} (Kanpur, India [dry season]). Ammonium nitrate ranged from 0.2 μg m^{-3} (Mammoth Cave, in summer) to 6.8 μg m^{-3} (Kanpur, dry season). Equivalent black carbon ranged from 0.7 μg m^{-3} (Mammoth Cave) to over 8 μg m^{-3} (Dhaka, Bangladesh and Kanpur, India). Comparison of SPARTAN versus coincident measurements from the Interagency Monitoring of Protected Visual Environments (IMPROVE) network at Mammoth Cave yielded a high degree of consistency for daily PM$_{2.5}$ (r^2 = 0.76, slope = 1.12), daily sulfate (r^2 = 0.86, slope = 1.03) and mean fractions of all major PM$_{2.5}$ components (within 6%). Major ions generally agree well with previous studies at the same urban locations (e.g. sulfate fractions agree within 4% for eight out of 11 collocation comparisons). Enhanced anthropogenic dust fractions in large urban areas (e.g. Singapore, Kanpur, Hanoi and Dhaka) are apparent from high Zn:Al ratios.

The expected water contribution to aerosols is calculated via the hygroscopicity parameter κ_v for each filter. Mean aggregate values ranged from 0.15 (Ilorin) to 0.28 (Rehovot). The all-site parameter mean is 0.20 ± 0.04. Chemical composition and water retention in each filter measurement allows inference of hourly PM$_{2.5}$ at 35% relative humidity by merging with nephelometer measurements. These hourly PM$_{2.5}$ estimates compare favorably with a beta attenuation monitor (MetOne) at the nearby US embassy in Beijing, with a coefficient of variation r^2 = 0.67 (n = 3167), compared to r^2 = 0.62 when κ_v was not considered. SPARTAN continues to provide an open-access database of PM$_{2.5}$ compositional filter information and hourly mass collected from a global federation of instruments.

1. Introduction

Fine particulate matter with a median aerodynamic diameter less than, or equal to, 2.5 µm ($PM_{2.5}$), is a robust indicator of premature mortality (Chen et al., 2008; Laden et al., 2006). Research on long-term exposure to ambient $PM_{2.5}$ has documented serious adverse health effects, including increased mortality from chronic cardiovascular disease, respiratory disease, and lung cancer (WHO, 2005). Outdoor fine particulate matter ($PM_{2.5}$) is recognized as a significant air pollutant, with an Air Quality Guideline set by the WHO at 10 µg m^{-3} annual average (WHO, 2006). Many regions of the world far exceed these long-term recommendations (Brauer et al., 2015; van Donkelaar et al., 2015), and the impact on health is substantial. The 2013 Global Burden of Disease estimated that outdoor $PM_{2.5}$ caused 2.9 million deaths (3 % of all deaths) and 70 million years of lost healthy life on a global scale (Forouzanfar et al., 2015). Atmospheric aerosol is also the most uncertain agent contributing to radiative forcing of climate change (IPCC, 2013). Aerosol mass and composition also play a critical role in atmospheric visibility (Malm et al., 1994). Additional observations are needed to improve the concentration estimates for $PM_{2.5}$ as a global risk factor, and to better understand the chemical components and sources contributing to its formation.

The chemical composition of $PM_{2.5}$ offers valuable information to identify the contributions of specific sources, and to understand aerosol properties and processes that could affect health, climate and atmospheric conditions. Spatial mapping of aerosol type and composition using satellite observations and chemical transport modelling can help elucidate the global exposure burden of fine particulate matter composition (Kahn and Gaitley, 2015; Lelieveld et al., 2015; Patadia et al., 2013; Philip et al., 2014a); however, ground-level sampling remains necessary to evaluate these estimates and provide quantitative detail. Furthermore, the long-term health impacts of specific chemical components are not well understood (e.g. Lepeule et al., 2012). The health-related impacts of specific PM composition have been reviewed previously (Lippmann, 2014). Although $PM_{2.5}$ composition can be implicated in the variance observed in cardiovascular health effects, there is insufficient long-term $PM_{2.5}$ characterization for adequate health impact assessments of specific aerosol mixtures (e.g. Bell et al., 2007). More generally, urban $PM_{2.5}$ speciation is not yet consistently characterized on a global scale. Continental sampling has been conducted in North America (Hand et al., 2012) and Europe (Putaud et al., 2004, 2010), however there remains a need for a global network that consistently measures $PM_{2.5}$ chemical composition in densely populated regions.

No global $PM_{2.5}$ protocol exists for relative humidity (RH) filter equilibration. The U.S. EPA measurements are between 30-40% RH, European measurements are below 50% RH, and different protocols exist elsewhere. Ambient humidity affects the relationship of dry $PM_{2.5}$ with satellite observations of aerosol optical depth. Aerosol water also influences the relationship between dry $PM_{2.5}$ and aerosol scatter. A large body of literature has examined the relationship of aerosol composition with hygroscopicity (e.g. IMPROVE (Hand et al., 2012; IMPROVE, 2015), Chemical Species Network (CSN) (Chu, 2004; USEPA, 2015), ISORROPIA (Fountoukis and Nenes, 2007), and Aerosol Inorganic Model (AIM) (Wexler and Clegg, 2002)). More recently Petters and Kreidenweis (2007, 2008, 2013) have developed κ-Kohler theory, which assigns individual hygroscopicity parameters κ to all major components, from insoluble crustal materials to sea-salt. Mixed values can then be weighted by local aerosol composition.

106
107	Ground-based observations of PM$_{2.5}$ have insufficient coverage at the global scale to
108	provide assessment of long-term human exposure. Satellite remote sensing offers a promising
109	means of providing an extended temporal record to estimate population exposure to PM$_{2.5}$ on a
110	global scale, and especially for areas with limited ground-level PM$_{2.5}$ measurements (Brauer et
111	al., 2015; van Donkelaar et al., 2015). Even in areas where monitor density is high, satellite-
112	based estimates provide additional useful information on spatial and temporal patterns in air
113	pollution (Kloog et al., 2011, 2013; Lee et al., 2012). However, there are outstanding questions
114	about the accuracy and precision with which ground-level aerosol mass concentrations can be
115	inferred from satellite remote sensing. Standardized PM$_{2.5}$ measurements, collocated with
116	ground-based measurements of aerosol optical depth, are needed to evaluate and improve PM$_{2.5}$
117	estimates from satellite remote sensing. To meet these sampling needs, the ground-based
118	network SPARTAN (Surface PARTiculate mAtter Network) is designed to evaluate and enhance
119	satellite-based estimates of PM$_{2.5}$ by measuring fine particle aerosol concentrations and
120	composition continuously over multi-year periods at sites where aerosol optical depth is also
121	measured (Holben et al., 1998; Snider et al., 2015). The network includes air filter sampling and
122	nephelometers that together provide long-term and hourly PM$_{2.5}$ estimates at low RH (35%).
123
124	We discuss the ongoing efforts of the SPARTAN project to quantify major ions and trace
125	metals found in aerosols worldwide. Section 2 describes the methodology used to infer PM$_{2.5}$
126	composition. Section 3 defines categories of aerosol types (crustal and residual material,
127	equivalent black carbon, ammonium nitrate, ammoniated sulfate, sea salt, and trace metal oxides)
128	as a function of specific chemical species. Section 4 describes the implementation of sub-
129	saturated κ-Kohler theory to estimate aerosol water content based on aerosol compositional
130	information. Section 5 compares relative aerosol composition with that reported in available
131	literature, and assesses the general consistency of our findings across all sites. Section 6
132	evaluates hourly PM$_{2.5}$ estimates (35% RH) at Beijing with a beta attenuation monitor at the US
133	Embassy.
134

2. Overview of Methodology

136
137	SPARTAN has been collecting PM$_{2.5}$ on PTFE filters for at least two months, across 13
138	SPARTAN sites, between 2013 and 2016, with an average period of 12 months per site. Snider
139	et al. (2015) provide an overview of the SPARTAN PM observation network, the cost-effective
140	sampling methods employed and post sampling instrumental methods of analysis. Each site
141	utilizes a combination of continuous monitoring by nephelometry and mass concentration via
142	filter-based sampling. Nephelometer scatter is averaged to hourly intervals at three wavelengths
143	(457 nm, 520 nm, 634 nm), and converted to 550 nm via a fitted Angstrom exponent. Total
144	scatter is proportional to PM$_{2.5}$ mass and volume (Chow et al., 2006). Hence we provide dry
145	(35% RH) hourly PM$_{2.5}$ estimates by combining scatter at 550 nm at ambient RH with filter mass
146	and chemical composition information used to determine water content as described below.
147
148	Briefly, filter-based measurements are collected with an AirPhoton SS4i automated air
149	sampler. Each sampler houses a removable filter cartridge that protects seven sequentially active
150	25 mm diameter filters plus a field blank. Air samples first pass through a bug screen and then a
151	greased impactor plate to remove particles larger than 10 μm in diameter. Aerosols are collected

152 in sequence on a preweighed Nuclepore filter membrane (8 μm, SPI) that removes coarse-mode
153 aerosols with diameters from 2.5 - 10 μm in diameter (PM_c), while fine aerosols ($PM_{2.5}$) are then
154 collected on pre-weighed PTFE filters (2 μm, SKC). For each filter, sampling is timed at regular,
155 staggered 24-hour intervals throughout a 9-day period. Sampling ends for each filter at 09:00
156 when temperatures are low, to reduce loss of semi-volatile components. As described by Snider
157 et al. (2015), loss rates of ammonium nitrate during passive air flow were an order of magnitude
158 less than during active air flow. Thus the sampling protocol is designed to actively sample for
159 one diurnal cycle and to avoid daytime sampling after collecting nighttime PM. Following the
160 IMPROVE protocol (Hand and Malm, 2006), filters are transported at room temperature in
161 sealed containers between measurement sites and the central SPARTAN laboratory at Dalhousie
162 University, where analysis is conducted.
163
164   Site locations are designed to sample under a variety of conditions, including biomass
165 burning (e.g. West Africa and South America), biofuel emissions (e.g. South Asia), monsoonal
166 conditions (e.g. West Africa and Southeast Asia), suspended mineral dust (e.g. West Africa and
167 the Middle East) and urban crustal material. Each SPARTAN site provides a representative
168 example of local and regional conditions in highly populated areas. Site selection prioritizes
169 under-represented globally-dispersed, population-dense regions; no SPARTAN sites yet exist in
170 Europe. The sites of Atlanta and Mammoth Cave are included for instrument inter-comparison
171 purposes with other networks.

172   ### 2.1. Filter weighing

173 Filters (PTFE, capillary) are both pre and post-weighed in triplicate using a Sartorius Ultramicro
174 balance with 0.1 μg precision. Gravimetric weighing is performed in a cleanroom facility at 35 ±
175 5% RH and 20-23°C. A total of 497 quality-controlled filters have been weighed across all
176 SPARTAN sites. The median collected material on sampled filters, as well as the lower and
177 upper quintiles (in parentheses), are 72 (42, 131) μg for Teflon and 90 (44, 154) μg for
178 Nuclepore. The combined uncertainty (± 2σ) of quality-assured single filter PM mass
179 measurements is ± 4.0 μg. Time-integrated flow rates at ambient air pressure and temperature are
180 used to define the sampled volume for aerosol concentrations reported in $μg/m^3$. These filters are
181 subsequently analyzed for water-soluble ions, trace metals, and surface reflectance to obtain
182 equivalent black carbon.

183   ### 2.2. Equivalent Black Carbon (EBC)

184 We define the equivalent black carbon (EBC) as the black carbon content of PTFE filters derived
185 via surface reflectance R using the Diffusion Systems Smoke Stain Reflectometer EEL 43M
186 (Quincey et al., 2009) as further discussed in Sect. 4.6. We use the term equivalent black carbon
187 following the recommendation of Petzold et al. (2013) for data derived from optical absorption
188 methods.

189   ### 2.3. Trace metals

190 To maximize the information extracted from the filters, each one is cut in half with a ceramic
191 blade following approaches similar to Zhang et al. (2013) and Gibson et al. (2009). One filter
192 half is analyzed for crustal components Mg, Fe, and Al as well as trace elements Zn, V, Ni, Cu,
193 As, Se, Ag, Cd, Sb, Ba, Ce and Pb. We first digest this filter half by adding it to 3.0 mL of 7%

194 trace metal grade nitric acid, similar to Fang et al. (2015). The acid/filter combination is boiled at
195 97C for 2 hours, and the liquid extract is submitted for quantitative analysis via inductively
196 coupled plasma mass spectrometry (ICP-MS, Thermo Scientific X-Series 2), and follows
197 standardized methodology as in Rice et al. (2012). The ICP-MS analysis is quantified via five
198 concentrations (25, 50, 100, 250, and 500 μg/L) of a 25-element acidified stock solution. Three
199 reference metal ions (^{45}Sc, ^{115}In, and ^{159}Tb) are also used for atomic mass calibration. All ion
200 mass signals are measured in triplicate, and the mean signal value is used for elemental
201 quantification.

2.4. Water soluble ions

203 Water-soluble ions NO_3^-, SO_4^{2-}, NH_4^+, K^+, Na^+ are detected using the second filter half. The filter
204 is spiked with 120 μL of isopropyl alcohol and immersed in 2.9 mL of 18 MΩ Milli-Q water.
205 Filters and liquid extracts are sonicated together for 25 min before being passed through a 0.45
206 μm membrane filter to remove larger matrix components. Extractions are analyzed by ion
207 chromatography (IC) via a Thermo Dionex ICS-1100 instrument (anions) and a Thermo Dionex
208 ICS-1000 (cations) instrument (Gibson et al., 2013a, 2013b).
209

3. PM$_{2.5}$ aerosol composition

211
212 Section 2 defined the methodology of basic physical and chemical properties obtained in
213 SPARTAN filters. Section 3 describes the chemical definitions used to infer each chemical
214 component as discussed in turn below. Table 1 contains a summary of equations and
215 accompanying references used to quantify SPARTAN PM$_{2.5}$ chemical composition.

3.1. Sea Salt (SS)

217 We take 10% of [Al] to be associated with Na and remove this crustal sodium component
218 (Remoundaki et al., 2013). Sea salt is then represented as 2.54[Na$^+$]$_{ss}$ to account for the
219 associated [Cl$^-$] (Malm et al., 1994).

3.2. Ammonium nitrate (ANO$_3$)

221 We treat all nitrate as neutralized by ammonium as NH$_4$NO$_3$. The corresponding mass of ANO$_3$
222 is a 1:1 molar ratio of NH$_4$:NO$_3$, or 1.29[NO$_3^-$] based on molecular weight.

3.3. Sodium sulfate (Na$_2$SO$_4$)

224 Sodium sulfate is treated as a fraction of measured sodium, 0.18[Na$^+$]$_{SS}$ (Henning et al., 2003);
225 however, it contributes negligibly to total aerosol mass (< 0.1%) at all sites.

3.4. Ammoniated sulfate (ASO$_4$)

227 Ammonium not associated with nitrate, and sulfate not associated with sodium, are assumed to
228 be associated as a mixture of NH$_4$HSO$_4$ and (NH$_4$)$_2$SO$_4$.

3.5. Crustal material (CM)

230 Crustal material consists of re-suspended road dust, desert dust, soil, and sand. Following the
231 elemental composition of natural desert dusts by Wang (2015), we generalize that natural CM is

232 approximately 10×[Al + Fe + Mg]. Aluminum, iron, and magnesium are chosen due to their
233 collectively consistent composition in natural mineral dust and frequency above detection limit
234 (> 95%). Silicon is not available. Titanium was found not to contribute significantly (< 1%) to
235 CM mass.

3.6. Equivalent Black Carbon (EBC)

237 The amount of EBC carbon (μg) is logarithmically related to concentration, as determined by
238 relative surface reflectance R/R_0. For a given exposed filter area, absorption cross-section and
239 light path, reflectance is related to concentration via

$$[\text{EBC}] = \frac{-A}{qv}\ln\left(\frac{R}{R_0}\right)$$ Eq. 1

240 where v is volume of air (0.9 to 5.8 m^3), A is the filter surface area (3.1 cm^2), and q is the product
241 of the effective reflectivity path p and mass-specific absorption cross section σ_{SSR} (cm^2/μg). The
242 absorption coefficient σ_{SSR} used here is 0.06 cm^2/μg based on prior literature (Barnard et al.,
243 2008; Bond and Bergstrom, 2006), adjusted to the 620 nm detection peak of the SSR. The
244 effective light path p here is taken to be 1.5 for our thick PTFE filters (e.g. Taha et al., 2007). We
245 treat water uptake by EBC as negligible.

3.7. Trace elemental oxides (TEO)

247 Trace elemental oxides are the summation of estimated oxide mass for trace elements as
248 measured by ICP-MS, and make up a negligible portion of total mass (< 1%). We include these
249 concentrations for completeness. Water uptake by TEO is treated as negligible.

3.8. Particle-bound water (PBW) associated with inorganics

251 We estimate the water-mass uptake for the inorganic chemical components of sea salt (SS),
252 ammonium nitrate (ANO$_3$) and ammoniated sulfate (ASO$_4$). The mass of particle-bound water
253 (PBW) associated with chemical component X is

$$PBW_X = [X]\kappa_{m,X}\frac{\text{RH}}{100-\text{RH}}$$ Eq. 2

254 The total mass of inorganic (IN) PBW is then PBW$_{IN}$= $\sum_X$ PBW$_X$.

3.9. Residual matter (RM)

256 Residual matter, which is treated as mainly organics, is estimated by subtracting dry inorganic
257 mass (IN) and its associated water (referenced to our weighing conditions of 35 ± 5 % RH) from
258 total PM$_{2.5}$ mass:

$$\text{RM}_{35\%} = \text{PM}_{2.5,35\%} - [\text{IN}] - [\text{PBW}_{IN}]$$ Eq. 3

259 Negative RM$_{35\%}$ values are retained if reconstructed inorganic mass at 35% RH exceeds total
260 PM$_{2.5}$ by less than 10%, otherwise values are flagged and excluded from the mass average.
261 Negative values occur, on average, 2% of the time. Water-free RM (0% RH) is estimated by
262 subtracting organic-associated PBW using an estimated hygroscopic parameter $\kappa_{m,RM}$ = 0.1 as
263 discussed in section 4.
264

4. Aerosol hygroscopicity

We apply the single-parameter measure of aerosol hygroscopicity (κ) developed by Petters and Kreidenweis (2007, 2008, 2013) to represent the contribution of water uptake by individual components. The κ parameter is defined from 0 (insoluble materials) to greater than 1 for sea salt. Although initially developed for supersaturated CCN conditions, hygroscopic parameters κ have been more recently used in sub-saturated conditions (Chang et al., 2010; Dusek et al., 2011; Giordano et al., 2013; Hersey et al., 2013). For particle diameters that dominate the mass fraction of PM$_{2.5}$ (larger than 50 nm), the difference in κ between CCN and sub-saturated aerosols is small (Dusek et al., 2011). The water retention of internal mixtures of aerosol components is often predicted within experimental error (Kreidenweis et al., 2008). Aged, polarized organic material, which is a major component of PM$_{2.5}$, shows comparable growth factors both in super- and sub-saturated regions (Rickards et al., 2013).

The volume hygroscopicity parameter κ_v is defined as a function of particle volume V and water activity a_w

$$\frac{1}{a_w} = 1 + \kappa_v \frac{V_d}{V_w} \qquad \text{Eq. 4}$$

where V_d and V_w are the dry particulate matter and water volumes, respectively. To a first-order approximation $a_w = $ RH/100. Aerosol volume growth is related via κ and RH by defining f_v(RH) as the humidity-dependent ratio of wet and dry aerosol volume:

$$f_v(\text{RH}) \equiv \frac{V_{tot}}{V_d} = \frac{V_d + V_w}{V_d} = a + \kappa_v \frac{\text{RH}}{100 - \text{RH}} \qquad \text{Eq. 5}$$

Combining the previous equations and relating to a diameter D growth factor ($GF \equiv D/D_d$) yields

$$GF = \left(a + \kappa_v \frac{\text{RH}}{100 - \text{RH}} \right)^{1/3} \qquad \text{Eq. 6}$$

where $a = 1$, except for sea salt as discussed in Sect. 3.1. Reliable estimates of κ_v are available for individual components (*c.f.* Table 2).

The next sections outline how we apply κ to represent mass and volume hygroscopic growth in major hygroscopic aerosol components. Four components directly contribute to water uptake: ammonium nitrate (ANO$_3$), ammoniated sulfate (ASO$_4$), sea salt (SS), and organics. We treat black carbon (EBC), crustal material (CM), and trace oxides (TEO) as non-hygroscopic. We evaluated inorganic component growth curves using the AIM model (Wexler and Clegg, 2002) for RH = 10 – 90% except for sea salt, which included RH = 0%. Hygroscopic parameters were matched to modeled fits. Aerosols are treated as internally mixed, without deliquescence or efflorescence points, as discussed further below.

4.1. Inorganic behavior

Figure 1 shows the hygroscopic growth for inorganics. The κ_v value of 0.51 for ammonium sulfate best matches the AIM model over RH = 10-90% and is similar to the *GF*-

299 derived $\kappa_v = 0.53$ estimated by Petters and Kreidenweis (2007). The κ_v value for ammonium
300 bisulfate is similar to the κ_v value of ammonium sulfate, which is adopted here for ASO$_4$ Our
301 AIM-derived ammonium nitrate growth curve is smaller than ammonium sulfate, at $\kappa_v = 0.41$.
302 Empirically both ammonium compounds share the same $GF = 1.6$ at RH = 85% (Sorooshian et
303 al., 2008), however ANO$_3$ is less hygroscopic at lower RH.
304
305　　　Sea salt accounts for a small fraction of aerosol mass over land, however its hydrophilic
306 nature makes it significant for water retention. A 1:1 volume ratio with water as RH approaches
307 0% (Kreidenweis et al., 2008) yields $a = 2$ (Eq. 2 and 3). A hygroscopic constant $\kappa_v = 1.5$ then
308 best fits AIM from the deliquescence point up to 90% RH.
309
310　　　We follow the widely used convention (e.g. Pitchford et al. (2007)) that PM$_{2.5}$ under
311 variable sub-saturated RH does not exhibit deliquescent phase transitions. There is compelling
312 evidence to adopt smooth hygroscopic growth curves. Various experiments show sub-
313 micrometer, internally mixed aerosols will not deliquesce as readily as pure compounds. For
314 example, Badger et al. (2006) observed ASO$_4$ aerosol deliquescence is clearly inhibited by the
315 presence of humic acids. A smooth growth curve has been observed over the range RH = 10 –
316 85% for ambient aerosols at Jungfraujoch (Swietlicki et al., 2008). Analysis of submicron aerosol
317 mixtures consisting of SS, ASO$_4$, ANO$_3$, and levoglucosan also showed no apparent phase
318 transition (Svenningsson et al., 2006).

319　　4.2. Organic matter behavior

320　　　Identifying a representative organic hygroscopic parameter is challenging, as many volume
321 growth curves are available based on a variety of laboratory experiments and field campaigns.
322 Organic composition varies by site, and by season. The Appendix table Al contains a collection
323 of hygroscopic parameters from the literature. Values for $\kappa_{v,OM}$ range from 0 to 0.2. We choose a
324 single $\kappa_{v,OM}$ value based on the oxygen/carbon ratio (O:C), which is a function of oxidation,
325 hence age of the organics. Generally O:C ratios are between 0.2 – 0.8 in urban environments
326 (Rickards et al., 2013). We select an O:C ratio of 0.5 to represent the populated nature of
327 SPARTAN sites (e.g. Robinson et al., 2013). This corresponds to an organic parameter of
328 $\kappa_{v,OM} = 0.1$ for a variety of organic mixtures (Jimenez et al., 2009).

329　　4.3. Aerosol water in multi-component systems

330　　　Mass-based hygroscopic water uptake κ_m is more convenient than κ_v to estimate water
331 retention in gravimetric analysis. The parameters κ_v and κ_m are related by water-normalized
332 density, $\kappa_{m,X} = \kappa_{v,X}/\rho_X$. Table 2 contains κ_v values identified for major aerosol chemical
333 components and densities. For a multi-component system we estimate aerosol water mass using a
334 mass-weighted combination of κ_m values:

$$\kappa_{m,tot} = \frac{1}{M} \sum_X m_X \kappa_{m,X} \qquad \text{Eq. 7}$$

335　　　Mass calculations are used to determine residual aerosol mass as described in Sect. 3.9.
336 Estimates of total water uptake by volume are applied to aerosol light scatter in Sect. 5. The
337 volume parameter $\kappa_{v,tot}$ is similarly determined by a linear combination of volume-weighted
338 components X (e.g. Bezantakos et al., 2013):

$$\kappa_{v,tot} = \frac{1}{V} \sum_X v_X \kappa_{v,X}$$ Eq. 8

339   The hygroscopic growth of ASO_4 and organic mixtures are treated as linear combinations of pure
340   compounds (Robinson et al., 2013). Errors in aerosol water uptake are less significant in mixtures
341   than for individual species due to dilution effects (Kreidenweis et al., 2008). For ambient aerosols,
342   empirically measured $\kappa_{v,tot}$ usually lies between 0.14 and 0.39 (Carrico et al., 2010).
343

344   ### 4.4. Sources of Uncertainty

345   Uncertainty in atmospheric $PM_{2.5}$ concentrations can be separated into air volume and $PM_{2.5}$
346   mass. We estimated total flow volume variance to be ± 10%, while 2σ pre and post gravimetric
347   mass measurement varied by a combined ± 4 μg. Characterization of hourly $PM_{2.5}$ uncertainties
348   can be found in Appendix A2.
349

350   Of concern is the loss of semivolatiles after sampling. In the laboratory semivolatile loss
351   is inhibited by storing filters in closed containers. As discussed in Section 2, the sampling
352   protocol is designed to minimize semi-volatile loss. We tested the retention of semivolatile
353   material in the field by examining the trend in $PM_{2.5}$ and ANO_3 mass from the first filter sampled
354   (54 day residence time in instrument) through the last filter sampled (negligible residence time in
355   instrument). Statistically insignificant trends were found for both $PM_{2.5}$ (-0.09 ± 0.46 μg m$^-$
356   ^{3}/position) and ANO_3 (0.06 ± 0.15 μg m^{-3}/position) providing confidence in retention of
357   semivolatiles on filters in the cartridge.
358

359   Other uncertainties include absolute equivalent black carbon mass due to the reflectivity
360   path p (± 30%) and absorption cross section σ (± 30%), which combine to in quadrature ± 42%.
361   Trace metal recovery yields were tested using a sequential second digestion with 20% nitric acid.
362   Each acid-digested element was quantified by five dilutions of a 25 element standard (25 – 500
363   *ppb*) plus three internal calibration metals (Sc, In, Tb). The elemental comparison of crustal
364   materials varies regionally (Wang, 2015), which contributes to CM uncertainty of ± 30% based
365   on Al, Fe and Mg composition. Recovery of individual water-soluble elements was determined
366   through 5-point anion and cation standards curves each with $r^2 > 98\%$ and <10% mass
367   uncertainty for most elements at environmentally-relevant concentrations, including sulfate,
368   nitrate, and ammonium. Based on lab filter spike tests, water-soluble ion extractions show > 95%
369   extraction efficiency. Uncertainties of water-soluble ion yields are generally ± 5%, except when
370   close to limit of detection (approximately 0.1 μg m^{-3}, depending on filter sampling duration).
371   Errors in the component values affect our estimate of κ_v, which will affect the inferred aerosol
372   water. Network evaluation is an ongoing task that will continue over time.
373

374 ## 5. Mass speciation results

375   ### 5.1. Overview of $PM_{2.5}$ mass speciation

376   Gravimetrically-weighed $PM_{2.5}$ concentrations within the period June 2013 to February 2016
377   span an order of magnitude, from under 10 μg m^{-3} (e.g. Atlanta) to almost 100 μg m^{-3} (Kanpur).

378   Sites include a variety of geographic regions including partial desert (Ilorin, Rehovot, Kanpur),
379   coastline (Buenos Aires, Singapore), and developing megacities (Dhaka). Table 3 and Figure 2
380   contain the resulting $PM_{2.5}$ mass, composition, and location of each SPARTAN site. The mean
381   SPARTAN composition over all sampling sites in descending concentration is 40% RM
382   (primarily organic), 20% ASO_4, 13% CM, 12% EBC, 4.7% ANO_3, 2.3% SS and 1.0% TEO.
383
384   There is significant variation of relative and absolute speciation from these long-term
385   averages. ASO_4 concentrations range from 1 $\mu g\ m^{-3}$ (Buenos Aires, summer) to 17 $\mu g\ m^{-3}$
386   (Kanpur, dry season). The fraction of sulfate in $PM_{2.5}$ exhibits much weaker spatial variation (10-
387   30%) as increases in ASO_4 coincide with increases in total $PM_{2.5}$. Hence locations with enhanced
388   sulfate tend to have enhancements in other aerosol components.
389
390   ANO_3 concentrations exhibit a larger spatial heterogeneity than sulfate. Absolute values
391   range over 30-fold, from 0.2 $\mu g\ m^{-3}$ (Mammoth Cave, summer) to 6.8 $\mu g\ m^{-3}$ (Kanpur, dry
392   season). Corresponding mass fractions are 7-8 % in Kanpur, Beijing, and Buenos Aires, and
393   below 2% in Bandung. This heterogeneity reflects large spatial and temporal variation in NH_3
394   and NO_x ($NO + NO_2$) sources. There were noticeable seasonal increases in ANO_3 during
395   wintertime periods in Beijing, Kanpur, and Dhaka, coinciding with lower temperatures.
396
397   CM concentrations span an order of magnitude from 1.0 $\mu g\ m^{-3}$ (Atlanta) to 16 $\mu g\ m^{-3}$
398   (Beijing). The fraction of CM in $PM_{2.5}$ exhibits pronounced variation (5-25%). Except during
399   dust storms, CM does not show clear patterns of temporal or regional variation. This could be
400   explained by non-seasonal road dust, which may account for over 80% of CM in regions with
401   heavy urban traffic (Huang et al., 2015).
402
403   We used Zn:Al ratios to assess the relative importance of local road dust (*c.f.* Table 3).
404   Aluminum is mostly natural in origin (Zhang et al., 2006) whereas Zn is primarily from tire wear
405   (Begum et al., 2010; Councell et al., 2004). For example, ratios are above 3 for Dhaka and
406   Hanoi, but less than 0.3 for Mammoth Cave and South Dekalb site (Atlanta). In fine-mode
407   aerosols, the ratio tends to be highest in large cities distant from natural CM. In coarse-mode
408   aerosols, a low Zn:Al ratio (< 0.1) indicates the aerosol CM component is dominated by regional
409   dust.
410
411   Absolute EBC spans an eight-fold concentration range from 1.1 $\mu g\ m^{-3}$ (Atlanta) to above 8
412   $\mu g\ m^{-3}$ (Dhaka and Kanpur). Mass fractions of EBC ranged from 4% (Singapore) to 25%
413   (Manila). Trace element oxide (TEO) material is mainly composed of Zn, Pb, Ni, Cu, and Ba,
414   hence also derived mainly from anthropogenic sources. TEO contributes negligibly to total mass
415   (1%), as expected. Sea salt remains a consistently small contributor (2%) to total mass, except
416   for Buenos Aires and Rehovot (5-6%) due to coastal winds. Particle-bound water (PBW) mass at
417   35% humidity is determined from the growth parameter κ_m. PBW mass contribution is similar to
418   EBC (7%). At low humidity, the combined mass of ANO_3, EBC, TEO, sea salt, and PBW
419   accounts for 15-35 % of aerosol mass.
420
421   RM as inferred from mass reconstruction of inorganic compounds, PBW, and total filter-
422   weighed mass is implicitly treated as the organic aerosol mass fraction. In terms of relative
423   composition, RM spans a factor of two, from 30% mass in Buenos Aires to almost 60% in

424　Kanpur. Temporal changes in RM tend to coincide with increases in ASO_4, with an all-site $r^2 =$
425　0.92. Although RM, as defined here, is not fully independent from measured ASO_4, correlations
426　between these two mass fractions imply related sources.
427
428　　　We interpret the abundance of water-soluble K relative to Al as an indicator of wood smoke
429　(e.g. Munchak et al., 2011). K:Al ratios averaged over each site range from < 2 (Mammoth Cave,
430　Atlanta) to 16 (Kanpur), where combustion activity is apparent. Singapore was downwind of
431　significant Indonesian forest fire smoke during its sampling period of Aug-Nov 2015, averaging
432　to K:Al = 13. The correlation between K:Al and RM across all SPARTAN sites is $r^2 = 0.73$,
433　supporting the attribution of RM as mostly organic.
434
435　　　Across all sites, coarse and fine mode mass fractions are approximately equal (0.50), with
436　fractions ranging from below 0.40 (Hanoi, Buenos Aires, and Manila) to above 0.55 (e.g.
437　Bandung, Kanpur, Atlanta, Mammoth Cave). The two size modes can be temporally correlated
438　per site, though sometimes weakly, from $r^2 = 0.15$ (Hanoi) to $r^2 = 0.76$ (Rehovot). We observe
439　strong temporal correlations between sulfate and ammonium in $PM_{2.5}$ ($r^2 = 0.72 - 0.99$). Nitrate
440　and ammonium are less consistently related (Table 3), ranging from higher values in Singapore
441　($r^2 = 0.66$), Kanpur ($r^2 = 0.58$), Beijing ($r^2 = 0.28$), to weaker values in Ilorin and Manila ($r^2 <$
442　0.1). The strength of correlations with ammonium could be influenced by excess ammonium
443　relative to sulfate. The $[NH_4^+]/[SO_4^{2-}]$ ratio in $PM_{2.5}$ is 2.6 in Kanpur and 1.3 in Ilorin.

444　　## 5.2. Collocation overview

445　　　We compare SPARTAN $PM_{2.5}$ speciation with previous studies available from the literature
446　and focus on collocated relative $PM_{2.5}$ composition of major components within the last 10 years.
447　TEO is omitted due to lack of significant mass contribution. Aerosol water content is also
448　omitted as it was not directly measured in any of the collocation studies. If not provided, CM is
449　treated as defined in Sect 4.5 where possible. Organic mass (OM) to organic carbon (OC) ratios
450　are from Philip et al. (2014b) with updates from Canagaratna et al. (2015).
451
452　　　Figure 3 provides an overview of the comparison studies organized by SPARTAN data
453　availability. Only sampling at Mammoth Cave sampling was temporally coincident with the
454　comparison data. SPARTAN compositional information is generally consistent with previous
455　studies, considering inter-annual chemical variation and measurement uncertainty. For example,
456　both SPARTAN and comparative studies find that $PM_{2.5}$ is composed of between 10-30% ASO_4
457　and 5-20% CM for sampled sites. SPARTAN EBC mass fraction generally matches within 5
458　percentage points of collocated studies, except for Bandung and Kanpur. SPARTAN and prior
459　studies find that ANO_3 is usually a small fraction of total mass, except at Beijing and Kanpur (7-
460　8%) due to their high agricultural and industrial activity. All studies find that sea-salt is below
461　3% of total mass. SPARTAN-derived RM has potentially the largest potential error, yet typically
462　is consistent with the combined organic and unknown masses of other studies. This offers further
463　evidence that SPARTAN measurements of RM are predominantly organic in nature.
464

465　　## 5.3. Individual site characteristics

466　　　Below we discuss each site in more detail. We also examine how our chemical composition
467　from a global array of sites relates to local anthropogenic activities and surrounding area.

468 References to land type at specific sites are derived from Latham et al. (2014), unless otherwise
469 indicated. The number of filters is given in parentheses.
470
471 ### 5.3.1 Beijing, China (n = 114)
472 Beijing has attracted considerable attention for its air pollution (Chen et al., 2013).
473 Agricultural areas to the west and the Gobi Desert to the north surround the city's 19 million
474 dwellers. The SPARTAN air sampler is located on the Tsinghua University campus, 15 km
475 northwest of the downtown center. This is our longest-running site, with 2.5 years of near-
476 continuous sampling. It reports the third-highest $PM_{2.5}$, at 69 μg m^{-3}, the third highest ASO_4 (12
477 μg m^{-3}) and the highest CM (16 μg m^{-3}) of all sites. The significant ANO_3 (5.5 μg m^{-3}) reflects
478 significant urban NO_x near agricultural NH_3 sources. ANO_3 values were highest during winter,
479 as expected from ammonium-nitrate thermodynamics. A high CM component in the springtime
480 reflects regional, natural CM sources. The mean $PM_{2.5}$ Zn:Al ratio is lower than in other large
481 cities (0.51) likely due to a larger fraction of natural dust sources and the sampling location in the
482 northwest quadrant of the city, upwind of many traffic sources. The lowest coarse-mode Zn:Al
483 mass ratios are observed in April 2014 (0.07) and April 2015 (0.06) during the annual Yellow
484 dust storm season. This is balanced by urban dust sources throughout the year, in agreement with
485 Lin et al. (2015) who found evidence of high CM in industrial areas of Beijing.
486
487 *Beijing Comparison:* Relative masses in Beijing compare well with previous studies.
488 SPARTAN ASO_4 (19%) is close to Yang et al. (2011) (17%) and Oanh et al. (2006) (20%)
489 and the RM of 37% is similar to combined OM (33 and 29%) and unknown fractions (10 and
490 24%) of comparison studies. SPARTAN ANO_3 concentrations (8.5%) are relatively higher
491 than for most other locations, though lower than in either previous study (11-12%), possibly
492 due to different sampling periods. CM is greater than in Yang et al. (2011) (25% vs. 19%),
493 and significantly higher than in Oanh et al. (2006) (5%), potentially due to a difference in
494 definitions.
495
496 ### 5.3.2 Bandung, Indonesia (n = 77)
497 Bandung is located inland on western Java surrounded by a volcanic mountain range and
498 agriculture (e.g. tea plantations). The sampler is located on the Institute of Technology Bandung
499 campus, 5 km north of the city center. Almost two years of sampling have resulted in a mean
500 $PM_{2.5}$ concentration of 31 μg m^{-3}. Sea salt is low at this elevated (826 m) inland site. ANO_3 and
501 CM levels are also low, but RM is moderately high compared with other sites, at 55%. This
502 could be explained by large amounts of vegetative burning; organic $PM_{2.5}$ mass fractions can rise
503 above 70% during combustion episodes (Fujii et al., 2014). Volcanic sources of sulfur, in
504 addition to industrial sources, may explain the relatively higher ASO_4 compared with Manila or
505 Dhaka (Lestari and Mauliadi, 2009). Influxes of volcanic dust from the Sinabang volcano from
506 August – September 2014 (2000 km northwest of Bandung) could explain why coarse-mode
507 Zn:Al ratios drop to 0.09 for this period compared to the annual mean of 0.21.
508
509 *Bandung Collocation:* Bandung is a volcanically active area, so that composition, in
510 particular ASO_4, differs due to naturally variable circumstances. SPARTAN ASO_4 (21%) is
511 higher than the 4% fraction reported by Lestari and Mauliadi (2009), but is identical with
512 measurements by Oanh et al. (2006). SPARTAN EBC (13%) is less than either previous
513 study (19% and 25%) and the more recent analysis of 19% BC (Santoso et al., 2013).

514   SPARTAN ANO_3 is 2% by mass, lower than measured by Oanh et al. (2006) (13%) but
515   similar to Lestari and Mauliadi (2009). Both of the earlier studies show lower RM fractions
516   (36%, and 42%) compared with 54% RM in this study.
517
518   *5.3.3 Manila, Philippines (n = 63)*
519   Manila is a coastal city located in Manila Bay, adjacent to the South China Sea and
520 surrounded by mountains. The sampling station, located at the Manila Observatory, is about 40
521 m higher in altitude than the central city. The $PM_{2.5}$ concentrations at the observatory (18 μg m^{-3})
522 are expected to be lower than in the main city, but still influenced by vehicular traffic, fuel
523 combustion and industry (Cohen et al., 2009). Compared to the all-site average, the CM fraction
524 in Manila is typical (11%), but equivalent black carbon is twice as great (25%). The high EBC
525 agrees with previous observations, attributable to a relatively high use of diesel engines (Cohen
526 et al., 2002).
527
528   *Manila Collocation:* SPARTAN fractions of ASO_4 and EBC are similar to Cohen et al.
529   (2009). Our RM (43%) is lower than OM (57%), whereas SPARTAN CM was greater than
530   Cohen et al. (2009). These differences could reflect sampling differences, or emission
531   changes over the last decade.
532
533   *5.3.4 Dhaka, Bangladesh (n = 41)*
534   Dhaka is a densely populated city (17,000 persons/km^2) in a densely populated country
535 (1,100 persons/km^2). The sampler is situated in the heart of downtown Dhaka, on the University
536 of Dhaka rooftop, and is influenced by air masses from the Indo Gangetic Plain (Begum et al.,
537 2012). More than half the country is used for agricultural purposes (Ahmed, 2013). Local
538 contributing $PM_{2.5}$ sources include coal and biomass burning, and heavy road traffic combustion
539 products and dust (Begum et al., 2010, 2012). $PM_{2.5}$ concentrations are the fourth highest of any
540 SPARTAN site, at 52 μg m^{-3}. Dhaka has the second-highest absolute EBC of any site, at 8.4 μg
541 m^{-3}, which can be explained by the abundance of truck diesel engines (Begum et al., 2012). We
542 estimate 41% of $PM_{2.5}$ in Dhaka is RM. Crop or bush burning on both local and regional scales
543 contribute significantly to organics (Begum et al., 2012). The high mean $PM_{2.5}$ Zn:Al ratio of 3.4
544 reflects a large contribution from urban traffic.
545
546   *5.3.5 Ilorin, Nigeria (n = 40)*
547   Ilorin is located in a rural area with low-level agriculture and shrub vegetation. The sampler
548 is sited on the university campus, 15 km east of the city of 500,000 people. Aerosol loadings
549 have seasonal cycles from agricultural burning events and dust storms (Generoso et al., 2003).
550 The RM accounted for two thirds of total $PM_{2.5}$ mass, among the largest, influenced by biomass
551 burning. There is evidence of biomass burning in the $PM_{2.5}$ peak in late spring 2014, and again in
552 2015. Lower ASO_4 (12%) compared to other SPARTAN sites reflects the sparse surrounding
553 industry. CM levels are comparable to other locations, except during dust storms. During a dust
554 storm (between April 14th - May 2nd 2015), CM increased to two thirds of $PM_{2.5}$ mass. The PM_c
555 Zn:Al ratio during the storm decreased to 0.01 versus 0.25 during non-storm days.
556
557   *5.3.6 Kanpur, India (n = 33)*
558   Kanpur is a city of 2.5 million people. The sampler is located at the IIT Kanpur campus
559 airstrip, about 10 km northwest of the city. The city lies in the Indo-Gangetic Plain, where

14

560 massive river floodplains are used for agricultural and industrial activity (Ram et al., 2012). We
561 sampled from December 2013 – May 2014, and September-November 2014, capturing one dry
562 season. SPARTAN-measured $PM_{2.5}$ for this period was 99 μg m^{-3}, the highest of any SPARTAN
563 site, of which 59% is RM, 19% ASO_4, and 7.4% ANO_3. The absolute values of all three
564 components are also the highest among those measured. Molar $[NH_4^+]:[SO_4^{2-}]$ ratios are higher
565 in Kanpur (2.6) than elsewhere. High background ammonia has been observed in the region
566 from satellite (e.g. Clarisse et al., 2009) which could explain the high levels of ANO_3. Wood
567 smoke is apparent from the high K:Al ratio (16), associated with organic matter burning during
568 winter dry months. We detected significant Zn concentrations (Zn:Al = 1.0), which is in
569 agreement with Misra et al. (2014) observations of a tripling of zinc during anthropogenic
570 sourced dust.
571
572 *Kanpur Collocation:* Relative fractions among the major species CM, sea salt, ASO_4 &
573 ANO_3 all match well with previous studies (Behera and Sharma, 2010; Chakraborty et al.,
574 2015; Ram et al., 2012) that also sampled during winter dry seasons. Chakraborty et al.
575 (2015) measured 70% organic mass composition and found a combined mass of 28% for
576 $ASO_4 + ANO_3$ compared to SPARTAN mass (26%). SPARTAN ASO_4 (19%) compares well
577 to 13% of Ram et al. (2012) and 18% for Behera and Sharma (2010), and ANO_3 (7.4%) is
578 close to previous values (6.1% and 6.6%). By comparison SPARTAN slightly overestimates
579 EBC by 4-6%. SPARTAN CM (4.8%) is lower than Behera and Sharma (2010) (10%).
580 Notably the combined OM + unknown fractions from these previous two studies account for
581 almost two thirds of aerosol mass, 58% for Behera and Sharma (2010) and 63% for Ram et
582 al. (2012), similar to our 59% RM estimate. SPARTAN $PM_{2.5}$ concentrations, as well as RM,
583 reach a maximum during the month of December. This is consistent with recent work
584 (Villalobos et al., 2015), who attribute this increase to agricultural burning and stagnant air.
585
586 ### 5.3.7 Buenos Aires, Argentina (n = 31)
587 Buenos Aires has a metropolitan population of 12 million. SPARTAN instruments are
588 located on the urban CITEDEF campus 20 km west of the central downtown. The megacity, the
589 southernmost in our study, is surrounded by grassland and farming on the west and the Atlantic
590 Ocean on the east. The latter explains the relatively high proportion (6%) of sea salt. Total $PM_{2.5}$
591 (10 μg m^{-3}) and relative RM (31%) are low compared with other large metropolitan areas, likely
592 influenced by clean maritime air. In addition to sea salt and natural CM, the contribution of EBC
593 is 17%, which could reflect significant local truck diesel combustion (Jasan et al., 2009).
594
595 ### 5.3.8 Rehovot, Israel (n = 30)
596 Rehovot is located on a four-story rooftop on the Weizmann Institute campus, 11 km from
597 the Mediterranean Sea and 20 km south of Tel Aviv. The city is surrounded by semi-arid, mixed-
598 use cropland, and the region experiences occasional Saharan desert dust outbreaks. Typical $PM_{2.5}$
599 concentrations are low (16 μg m^{-3}), with the composition in Rehovot consisting of 29% ASO_4,
600 and 20% CM. The RM fraction is smaller in Rehovot (16% total $PM_{2.5}$ mass) than at other
601 SPARTAN sites. Aerosol sources in Israel include agriculture, desert dust, traffic and coal-based
602 power plants (Graham et al., 2004). Relative sodium concentrations are high in Rehovot (4%),
603 similar to Buenos Aires and Ilorin, and may include a contribution from dust.
604

605   *Lag Ba'Omer festival:* We measured high ASO_4 concentrations on May 7-18, 2015, during
606   which time a large number of bonfires were lit nearby. During the festival, over 75% of total
607   aerosol mass came from $ASO_4 + ANO_3$, leading to a brief doubling of the hygroscopic
608   parameter κ_v. We observed a K:Al ratio of 38 for May 6th of the festival, the highest for any
609   single filter.
610
611   *Saharan dust storm:* We had the opportunity to measure a severe dust storm in Rehovot from
612   a filter sampling February 4-13, 2015. The coarse filter Zn:Al ratio dropped to 0.02 during
613   the Saharan dust storm from the typical value of 0.3. On the coarse filter we obtained an
614   absolute CM mass of 950 μg, which accounts for half of the collected mass during the storm.
615   13% of dust storm PM_c is combined sea salt, ANO_3, and ASO_4, leaving 35% RM. Although
616   this RM fraction may imply an incomplete CM extraction, it is possible that a significant
617   portion of desert dust carries adsorbed organic material (Falkovich et al., 2004).
618
619   ### 5.3.9 Mammoth Cave NP, US (n = 19)
620   The Mammoth Cave sampling site straddles National Park mountainous terrain to the north
621   and east, with farmland to the south and west. It is about 35 km from the closest town, Bowling
622   Green, KY, with about 50,000 residents. Sources of PM are expected to be non-local, hence we
623   consider it our 'background' site.
624
625   *Mammoth Cave National Park Collocation*: This temporary SPARTAN site was deployed
626   for comparison with the IMPROVE network station (IMPROVE, 2015). Unique among our
627   sites, sampling was temporally coincident with IMPROVE's 1-in-3 day regimen. We
628   obtained quality-controlled samples from June-August 2014. Temporal variation in daily
629   values is consistent with IMPROVE for sulfate ($r^2 = 0.86$, slope = 1.03) and total mass of
630   $PM_{2.5}$ ($r^2 = 0.76$, slope = 1.12). Differences between IMPROVE vs. SPARTAN are small for
631   ASO_4 (36% vs. 33%), ANO_3 (2.4% vs. 1.2%), CM (7% vs. 11%), and EBC (3.0% vs. 5.6%),
632   respectively. The combined OM + unknown + water fraction IMPROVE was 51%, similar to
633   the SPARTAN RM mass fraction of 49%.
634
635   ### 5.3.10 Atlanta, US (n = 13)
636   Atlanta represents a major urban area in a developed country. The temporary SPARTAN site
637   was located at the South Dekalb supersite 15 km east of downtown Atlanta. Air sampling was
638   performed for a 4-month period spanning winter to spring 2014. Over the past 10 years
639   significant decreases in $PM_{2.5}$ have been observed here and across the eastern United States
640   (Boys et al., 2014). The surrounding region is tree-covered or agricultural.
641
642   *Atlanta (South Dekalb) Collocation:* Co-sampled filters from the Atlanta CSN station
643   (USEPA, 2015) provide a comparison with the summer 2014 SPARTAN data. The EPA OM
644   fraction (43%) agrees well with the SPARTAN mean RM (48%). Crustal, SS, EBC and
645   ASO_4 are within 2% relative to total composition. SPARTAN component fractions in Atlanta
646   are also consistent with respect to Butler et al. (2003); components CM (12% vs. 10%),
647   ASO_4 (23% vs. 28%), ANO_3 (3.5% vs 4%) and RM and OM (48% vs 55%) closely match,
648   except for EBC (11% vs. 3%), perhaps reflecting different time periods.
649
650   ### 5.3.11 Singapore, Singapore (n = 12)

651   Singapore is a densely populated coastal city-state at 7,770 people/km^2. The sampler is
652 located on a rooftop at the National University of Singapore (NUS), near the center of the city.
653 Transportation is mixed-use, including taxis, rail, and bicycles, which may help explain the
654 relatively low EBC and CM of 3%. Despite this, the Zn:Al ratio remains high at 1.5, implying a
655 dominant traffic-based contribution to CM. SPARTAN instruments have observed significant
656 biomass burning downwind from Indonesia, causing an increase in absolute PM$_{2.5}$ from 32 in
657 August to 120 μg m^{-3} in September 2015, as well as an increase in RM from 44% to 62%. The
658 K:Al ratio steadily increased during this same period, from 7.2 (Jul 24 – Aug 2, 2015) to 17 – 24
659 (Aug 11 – Sept 25).

660
661

662   ***5.3.12 Hanoi, Vietnam (n = 10)***
663   Hanoi is an inland megacity surrounded by grassland and agriculture. The sampler itself is on
664 a building rooftop at the Vietnam Academy of Science and Technology, 5 km northwest of the
665 city center. Motorbikes are the main forms of transportation downtown and the primary source of
666 mobile-based PM$_{2.5}$ (Vu Van et al., 2013). In Hanoi, the PM$_{2.5}$ Zn:Al ratio was 3.7, also the
667 highest of any SPARTAN site, indicative of significant traffic and tire wear.

668
669   *Hanoi Comparison:* SPARTAN PM$_{2.5}$ composition is generally consistent with Cohen et al.
670   (2010). Slight differences are perhaps related to differences in sampling season and location.
671   SPARTAN sea salt fraction was larger (2.5% vs. 0.6%), but with a lower ASO$_4$ fraction
672   (17%) compared with Cohen et al. (2010) (29%). Sulfate tends to be lower in the spring-
673   summer seasons, coinciding with our measurement period, which may explain the
674   discrepancy. SPARTAN EBC (10%) is close to the Cohen et al. (2010) value of 8%, whereas
675   SPARTAN RM (51%) and CM (16%) masses are slightly higher.

676
677   ***5.3.13 Pretoria, South Africa (n = 5)***
678   Pretoria is a high-altitude city (1300 m) surrounded by arid, low-intensity agriculture and
679 extensive grasslands. The SPARTAN sampler is located on a 10 m CSIR building rooftop 12 km
680 east of downtown area (*pop.* 700,000). Preliminary measurements of south-hemisphere
681 springtime show absolute PM$_{2.5}$ concentrations to be low, at 6.4 μg m^{-3}. There are significant
682 fractions of CM (22%) and EBC (22%), and low RM (14%). The PM$_{2.5}$ Zn:Al ratio (0.69)
683 indicates vehicle traffic contributes to CM.

684 ## 6. Refining estimates of dry hourly PM$_{2.5}$ using κ_v

685 Our assessment of PM$_{2.5}$ hygroscopicity is determined by site-specific chemical composition. We
686 then use the time-varying hygroscopicity to refine the PM$_{2.5}$ values inferred from nephelometer
687 scatter.

688   ### 6.1. Relating PM$_{2.5}$ composition to κ_v

689   The outer pie charts of Figure 2 show the site-mean hygroscopic growth constant κ_v,
690 surrounded by the water contributions at 35% RH. The major contributors to PBW are ASO$_4$,
691 ANO$_3$, RM, and sea salt, as inferred from the values listed in Table 2 and weighted by
692 composition as in Eq. 5. ASO$_4$ and RM contribute similarly to total aerosol water whereas ANO$_3$
693 contributes less to PM$_{2.5}$ hygroscopicity due to its smaller mass. The contribution of sea salt to

694 hygroscopicity can be significant, and makes a dominant contribution in both Rehovot and
695 Buenos Aires.
696
697   The parameter κ_v, when averaged across all sites, is 0.20, matching the generic estimate
698 $\kappa_{v,tot}$ = 0.2 applied in the initial SPARTAN study (Snider et al., 2015). Recently Brock et al.
699 (2016) estimate κ_v values between 0.15 and 0.25 for ambient aerosols with 50% organic
700 composition at subsaturated humidity. The local SPARTAN value in Atlanta (0.17) is consistent
701 with the value of 0.16 ± 0.07 by Padró et al. (2012) in Atlanta. We found significant long-term
702 differences in $\kappa_{v,tot}$ between cities, from 0.15 in Ilorin to 0.28 in Rehovot, and differences
703 between filters at single sites (σ ∼ 0.05). There is little correlation of $\kappa_{v,tot}$ with changes in mass
704 (r^2 < 0.01). However, there are significant changes in $\kappa_{v,tot}$ due to seasonality and specific
705 events (e.g. dust storms, fires). In Beijing, aerosol hygroscopicity was 50% higher in mid
706 summer (August) due to increased sulfate, and in late winter (March) due to a relative increase in
707 sea salt. A summertime sulfate peak also agrees with observations by Yang et al. (2011). Table 3
708 shows the site-specific PBW in PM$_{2.5}$. At RH =35%, PBW ranges from $0.6 - 6$ μg m^{-3},
709 comparable in absolute values to EBC. Above 80% RH PBW will account for more than half of
710 aerosol mass. Accounting for this water component in nephelometer scatter motivates the
711 following section.

712   6.2. Relating nephelometer scatter to dry (RH=35%) PM$_{2.5}$

713 We apply a temporally resolved, site-specific κ_v to refine our relationship between total
714 nephelometer scatter and PM$_{2.5}$. We calculate a 45-day running mean aerosol volume-weighted
715 κ_v at each SPARTAN site. We then use the hygroscopic growth factors to estimate dry hourly
716 PM$_{2.5}$ from hourly nephelometer measurements of ambient scatter and hourly measured RH.
717 Appendix A2 describes the procedure in more detail.
718
719   We compared our hourly PM$_{2.5}$ in Beijing with PM$_{2.5}$ measurements from a Beta Attenuation
720 Monitor (BAM, MetOne) at the US Embassy, located 15 km away. The BAM instrument
721 contains a drying column with a 35% humidity set point. The left panel of Figure 4 shows the
722 time series of hourly dry PM$_{2.5}$ concentrations predicted by SPARTAN during the summer.
723 Pronounced temporal variation is apparent, with PM$_{2.5}$ concentrations varying by more than an
724 order of magnitude. A high degree of consistency is found with the BAM ($r^2 = 0.67$). The
725 exclusion of water uptake in hourly PM$_{2.5}$ estimates (by setting all $\kappa_v = 0$) decreased hourly
726 correlations slightly to $r^2 = 0.62$. The average humidity in Beijing was 47% for the measurement
727 period, corresponding to a mean 17% volume contribution by water ($\kappa_v = 0.19$). Hygroscopic
728 growth should play a more significant role under more humid conditions (e.g. Manila and
729 Dhaka).
730
731   The right panel in Figure 4 shows daily-averaged PM$_{2.5}$ ($n = 148$). In 2014 there were 3167
732 coincidentally available hours with which to compare. The coefficient of variation for averaged
733 24-hour measurements remained high ($r^2 = 0.70$). There was a mean offset of 10 μg m^{-3}.
734 However the slope is near unity (0.98), suggesting excellent proportionality between our
735 nephelometer and the BAM instrument for PM$_{2.5}$ concentrations below 200 μg m^{-3}. Above this
736 concentration, nephelometer signals become non-linear. The agreement remained similar for
737 hourly values ($r^2 = 0.67$).

18

738

7. Conclusions

740

We have established a multi-country network where continuous monitoring with a 3-wavelength nephelometer is combined with a single multi-day composite filter sample to provide information on $PM_{2.5}$. Long-term average aerosol composition is inferred from the filters, including equivalent black carbon, sea salt, crustal material, ammoniated sulfate, and ammonium nitrate. This composition information was applied to calculate aerosol hygroscopicity, and in turn the relation between aerosol scatter at ambient and controlled RH. These data provide a consistent set of compositional measurements from 13 sites in 11 countries.

748

We report ongoing measurements of fine particulate matter ($PM_{2.5}$), including compositional information, in 13 locations in two month or greater intervals all within a three-year span (2013-2016). The mean composition averaged for all SPARTAN sites is ammoniated sulfate (20% ± 11%), crustal material (13.4% ± 9.9%), equivalent black carbon (11.9% ± 8.4%), ammonium nitrate (4.7% ± 3.0%), sea salt (2.3% ± 1.6%), trace element oxides (1.0% ± 1.1%), water (7.2% ± 3.3%) at 35% RH, and residual matter, which is probably primarily organic (40% ± 24%).

755

Analysis of filter samples reveals that several $PM_{2.5}$ chemical components varied by more than an order of magnitude between sites. Ammoniated sulfate ranged from 1 μg m^{-3} in Buenos Aires to 17 μg m^{-3} in Kanpur (dry season). Ammonium nitrate ranged from 0.2 μg m^{-3} (Mammoth Cave, summertime) to 6.8 μg m^{-3} (Kanpur, dry season). Equivalent black carbon ranged from 0.7 μg m^{-3} (Mammoth Cave) to 8 μg m^{-3} (Dhaka and Kanpur). Locations with enhanced sulfate tend to have enhancements in other PM components. For example, ammoniated sulfate and residual matter (probably organic) are highly correlated across sites ($r^2 = 0.92$).

763

Crustal material concentrations ranged from 1 μg m^{-3} (Atlanta) to 16 μg m^{-3} (Beijing). Measuring Zn:Al ratios in $PM_{2.5}$ was an effective way to determine anthropogenic contribution to crustal material. Ratios larger than 0.5 identified sites with significant road dust contributions (e.g. in Hanoi, Dhaka, Manila, and Kanpur). Some locations, such as Beijing and Buenos Aires, had both high anthropogenic and natural crustal material. Low coarse Zn:Al ratios were apparent during natural dust storms. Anthropogenic crustal material is an aerosol component neglected by most global models and which may deserve more attention.

771

Potassium is a known marker for wood smoke. Enhanced K:Al ratios were found in Singapore downwind of Indonesian forest fires, in Kanpur during the winter dry season from agricultural burning, and in Rehovot during a bonfire festival. Furthermore, these ratios were correlated with RM concentrations ($r^2 = 0.73$), supporting the attribution of RM as mostly organic.

777

SPARTAN measurements generally agree well with previous collocated studies. SPARTAN sulfate fractions are within 4% of fractions measured at eight of the ten collocated, though temporally non-coincident, studies. Dedicated contemporaneous collocation with IMPROVE at Mammoth Cave yielded a high degree of consistency with daily sulfate ($r^2 = 0.86$, slope = 1.03), daily $PM_{2.5}$ ($r^2 = 0.76$, slope = 1.12), and mean fractions for all major $PM_{2.5}$ components (within

783　2%). Crustal material is typically consistent with the previous measurements, at 5-15%
784　composition. SPARTAN equivalent black carbon ranged broadly, from 3% (Singapore) to 25%
785　(Manila), and matched within a few percent of most previous works. Ammonium nitrate (4%)
786　generally matched other sites, though it was sometimes lower, as in Beijing and Atlanta. Sea-salt
787　was consistently low, as found in previous measurements. Sea salt fractions were highest in
788　Buenos Aires and Rehovot (6%), reflecting natural coastal aerosols. SPARTAN residual matter
789　is consistent with the combined organic and unknown masses. Comparing with collocated
790　measurements supports the expectation that most of the RM is partially organic. Residual matter
791　could also include unaccounted-for particle bound water, measurement error, and possibly
792　unmeasured inorganic materials.
793
794　　　　We calculated the hygroscopic constant κ_v for individual $PM_{2.5}$ filters to estimate water at
795　variable humidity, and to infer wet and water-free residual matter. Based on a range of literature,
796　we treated residual matter as mostly organic, with constant $\kappa_{v,RM} = 0.1$. Residual matter and
797　ammoniated sulfate largely determined overall water uptake in aerosols. These individual
798　species, along with sea salt and ammonium nitrate, resulted in a mean mixed hygroscopic
799　constant of 0.20, implying that for many sites, water content above 80% RH will account for
800　more than half of aerosol mass. For cleanroom conditions of low humidity (35% RH), mean
801　water composition was estimated to be 7% by mass.
802
803　　　　Water retention calculations allow for volumetric fluctuation estimates of aerosol water at
804　variable RH. We subtracted the water component to predict dry nephelometer scatter as a
805　function of time, anchored to filter masses at 35% RH. For Beijing, we assessed the consistency
806　of SPARTAN predictions of hourly $PM_{2.5}$ values with BAM measurements taken 15 km away,
807　and found temporal consistency ($r^2 = 0.67$), with a slope near unity (0.98). The explained
808　variance decreased to $r^2 = 0.62$ when setting $\kappa_v = 0$. This comparison tested both SPARTAN
809　instrumentation and our treatment of aerosol water uptake.
810
811　　　　These measurements provide chemical and physical data for future research on $PM_{2.5}$.
812　Collocation with sun photometer measurements of AOD connects satellite observations to
813　ground-based measurements and provides information needed to evaluate chemical transport
814　model simulations of the $PM_{2.5}$ to AOD ratio. As sampling expands, SPARTAN will provide
815　long-term data on fine aerosol variability from around the world. Ongoing work includes an
816　analysis of trace metal concentrations and interpreting SPARTAN measurements with a
817　chemical transport model. The data are freely available as a public good at www.spartan-
818　network.org. We welcome expressions of interest to join this grass-roots network.
819
820

Acknowledgements

8. References

Ahmed, S.: Food and Agriculture in Bangladesh, Encycl. Food Agric. Ethics, doi:10.1007/978-94-007-6167-4_61-2, 2013.

Asa-Awuku, A., Moore, R. H., Nenes, A., Bahreini, R., Holloway, J. S., Brock, C. A., Middlebrook, A. M., Ryerson, T. B., Jimenez, J. L., DeCarlo, P. F., Hecobian, A., Weber, R. J., Stickel, R., Tanner, D. J. and Huey, L. G.: Airborne cloud condensation nuclei measurements during the 2006 Texas Air Quality Study, J. Geophys. Res. Atmos., 116(D11), D11201, doi:10.1029/2010JD014874, 2011.

Badger, C. L., George, I., Griffiths, P. T., Braban, C. F., Cox, R. A. and Abbatt, J. P. D.: Phase transitions and hygroscopic growth of aerosol particles containing humic acid and mixtures of humic acid and ammonium sulphate, Atmos. Chem. Phys., 6(3), 755–768, doi:10.5194/acp-6-755-2006, 2006.

Barnard, J. C., Volkamer, R. and Kassianov, E. I.: Estimation of the mass absorption cross section of the organic carbon component of aerosols in the Mexico City Metropolitan Area, Atmos. Chem. Phys., 8(22), 6665–6679, doi:10.5194/acp-8-6665-2008, 2008.

Begum, B. A., Biswas, S. K., Markwitz, A. and Hopke, P. K.: Identification of sources of fine and coarse particulate matter in Dhaka, Bangladesh, Aerosol Air Qual. Res., 10, 345–353, doi:10.4209/aaqr.2009.12.0082, 2010.

Begum, B. A., Hossain, A., Nahar, N., Markwitz, A. and Hopke, P. K.: Organic and black carbon in PM2.5 at an urban site at Dhaka, Bangladesh, Aerosol Air Qual. Res., 12(6), 1062–1072, 2012.

Behera, S. N. and Sharma, M.: Reconstructing primary and secondary components of PM2.5 composition for an urban atmosphere, Aerosol Sci. Technol., 44(11), 983–992, doi:10.1080/02786826.2010.504245, 2010.

Bell, M. L., Dominici, F., Ebisu, K., Zeger, S. L. and Samet, J. M.: Spatial and temporal variation in PM2.5 chemical composition in the United States for health effects studies, Environ. Health Perspect., 115(7), 989–995, doi:10.2307/4619499, 2007.

Bezantakos, S., Barmpounis, K., Giamarelou, M., Bossioli, E., Tombrou, M., Mihalopoulos, N., Eleftheriadis, K., Kalogiros, J., D. Allan, J., Bacak, A., Percival, C. J., Coe, H. and Biskos, G.: Chemical composition and hygroscopic properties of aerosol particles over the Aegean Sea, Atmos. Chem. Phys., 13(22), 11595–11608, doi:10.5194/acp-13-11595-2013, 2013.

Bond, T. C. and Bergstrom, R. W.: Light absorption by carbonaceous particles: an investigative review, Aerosol Sci. Technol., 40(1), 27–67, doi:10.1080/02786820500421521, 2006.

Boys, B. L., Martin, R. V, van Donkelaar, A., MacDonell, R. J., Hsu, N. C., Cooper, M. J., Yantosca, R. M., Lu, Z., Streets, D. G., Zhang, Q. and Wang, S. W.: Fifteen-year global time series of satellite-derived fine particulate matter, Environ. Sci. Technol., 48(19), 11109–11118, doi:10.1021/es502113p, 2014.

Brauer, M., Freedman, G., Frostad, J., van Donkelaar, A., Martin, R. V, Dentener, F., Dingenen, R. van, Estep, K., Amini, H., Apte, J. S., Balakrishnan, K., Barregard, L., Broday, D., Feigin, V., Ghosh, S., Hopke, P. K., Knibbs, L. D., Kokubo, Y., Liu, Y., Ma, S., Morawska, L., Sangrador, J. L. T., Shaddick, G., Anderson, H. R., Vos, T., Forouzanfar, M. H., Burnett, R. T. and Cohen, A.: Ambient air pollution exposure estimation for the Global Burden of Disease 2013, Environ. Sci. Technol., doi:10.1021/acs.est.5b03709, 2015.

Brock, C. A., Wagner, N. L., Anderson, B. E., Attwood, A. R., Beyersdorf, A., Campuzano-Jost, P., Carlton, A. G., Day, D. A., Diskin, G. S., Gordon, T. D., Jimenez, J. L., Lack, D. A., Liao, J., Markovic, M. Z., Middlebrook, A. M., Ng, N. L., Perring, A. E., Richardson, M. S., Schwarz, J. P., Washenfelder, R. A., Welti, A., Xu, L., Ziemba, L. D. and Murphy, D. M.: Aerosol optical properties in the southeastern United States in summer – Part 1: Hygroscopic growth, Atmos. Chem. Phys., 16(8), 4987–5007, doi:10.5194/acp-16-4987-2016, 2016.

Butler, A. J., Andrew, M. S. and Russell, A. G.: Daily sampling of PM2.5 in Atlanta: results of the first year of the assessment of spatial aerosol composition in Atlanta study, J. Geophys. Res. Atmos., 108(D7), 8415, doi:10.1029/2002JD002234, 2003.

Canagaratna, M. R., Jimenez, J. L., Kroll, J. H., Chen, Q., Kessler, S. H., Massoli, P., Hildebrandt Ruiz, L., Fortner, E., Williams, L. R., Wilson, K. R., Surratt, J. D., Donahue, N. M., Jayne, J. T. and Worsnop, D. R.: Elemental ratio

885   measurements of organic compounds using aerosol mass spectrometry: characterization, improved calibration, and
886   implications, Atmos. Chem. Phys., 15(1), 253–272, doi:10.5194/acp-15-253-2015, 2015.

887   Carrico, C. M., Petters, M. D., Kreidenweis, S. M., Sullivan, A. P., McMeeking, G. R., Levin, E. J. T., Engling, G.,
888   Malm, W. C. and Collett, J. L.: Water uptake and chemical composition of fresh aerosols generated in open burning
889   of biomass, Atmos. Chem. Phys., 10(11), 5165–5178, doi:10.5194/acp-10-5165-2010, 2010.

890   Chakraborty, A., Bhattu, D., Gupta, T., Tripathi, S. N. and Canagaratna, M. R.: Real-time measurements of ambient
891   aerosols in a polluted Indian city: Sources, characteristics, and processing of organic aerosols during foggy and
892   nonfoggy periods, J. Geophys. Res. Atmos., 120(17), 2015JD023419, doi:10.1002/2015JD023419, 2015.

893   Chang, R. Y.-W., Slowik, J. G., Shantz, N. C., Vlasenko, A., Liggio, J., Sjostedt, S. J., Leaitch, W. R. and Abbatt, J.
894   P. D.: The hygroscopicity parameter (κ) of ambient organic aerosol at a field site subject to biogenic and
895   anthropogenic influences: relationship to degree of aerosol oxidation, Atmos. Chem. Phys., 10(11), 5047–5064,
896   doi:10.5194/acp-10-5047-2010, 2010.

897   Chen, H., Goldberg, M. S. and Villeneuve, P. J.: A systematic review of the relation between long-term exposure to
898   ambient air pollution and chronic diseases., Rev. Environ. Health, 23(4), 243–297, 2008.

899   Chen, Z., Wang, J.-N., Ma, G.-X. and Zhang, Y.-S.: China tackles the health effects of air pollution, Lancet,
900   382(9909), 1959–1960, 2013.

901   Chow, J. C., Watson, J. G., Park, K., Lowenthal, D. H., Robinson, N. F. and Magliano, K. A.: Comparison of
902   particle light scattering and fine particulate matter mass in central California., J. Air Waste Manage. Assoc., 56(4),
903   398–410, 2006.

904   Chu, S.-H.: PM2.5 episodes as observed in the speciation trends network, Atmos. Environ., 38(31), 5237–5246,
905   doi:10.1016/j.atmosenv.2004.01.055, 2004.

906   Clarisse, L., Clerbaux, C., Dentener, F., Hurtmans, D. and Coheur, P.-F.: Global ammonia distribution derived from
907   infrared satellite observations, Nat. Geosci, 2(7), 479–483, 2009.

908   Cohen, D. D., Garton, D., Stelcer, E., Wang, T., Poon, S., Kim, J., Oh, S. N., Shin, H.-J., Ko, M. Y. and Santos, F.:
909   Characterisation of PM2. 5 and PM10 fine particle pollution in several Asian regions., 2002.

910   Cohen, D. D., Stelcer, E., Santos, F. L., Prior, M., Thompson, C. and Pabroa, P. C. B.: Fingerprinting and source
911   apportionment of fine particle pollution in Manila by IBA and PMF techniques: A 7-year study, X-Ray Spectrom.,
912   38(1), 18–25, doi:10.1002/xrs.1112, 2009.

913   Cohen, D. D., Crawford, J., Stelcer, E. and Bac, V. T.: Characterisation and source apportionment of fine particulate
914   sources at Hanoi from 2001 to 2008, Atmos. Environ., 44(3), 320–328, doi:10.1016/j.atmosenv.2009.10.037, 2010.

915   Councell, T. B., Duckenfield, K. U., Landa, E. R. and Callender, E.: Tire-wear particles as a source of zinc to the
916   environment, Environ. Sci. Technol., 38(15), 4206–4214, doi:10.1021/es034631f, 2004.

917   Dabek-Zlotorzynska, E., Dann, T. F., Kalyani Martinelango, P., Celo, V., Brook, J. R., Mathieu, D., Ding, L. and
918   Austin, C. C.: Canadian National Air Pollution Surveillance (NAPS) PM2.5 speciation program: Methodology and
919   PM2.5 chemical composition for the years 2003–2008, Atmos. Environ., 45(3), 673–686, 2011.

920   Duplissy, J., DeCarlo, P. F., Dommen, J., Alfarra, M. R., Metzger, A., Barmpadimos, I., Prevot, A. S. H.,
921   Weingartner, E., Tritscher, T., Gysel, M., Aiken, A. C., Jimenez, J. L., Canagaratna, M. R., Worsnop, D. R., Collins,
922   D. R., Tomlinson, J. and Baltensperger, U.: Relating hygroscopicity and composition of organic aerosol particulate
923   matter, Atmos. Chem. Phys., 11(3), 1155–1165, doi:10.5194/acp-11-1155-2011, 2011.

924   Dusek, U., Frank, G. P., Massling, A., Zeromskiene, K., Iinuma, Y., Schmid, O., Helas, G., Hennig, T.,
925   Wiedensohler, A. and Andreae, M. O.: Water uptake by biomass burning aerosol at sub- and supersaturated
926   conditions: closure studies and implications for the role of organics, Atmos. Chem. Phys., 11(18), 9519–9532,
927   doi:10.5194/acp-11-9519-2011, 2011.

928   Falkovich, A. H., Schkolnik, G., Ganor, E. and Rudich, Y.: Adsorption of organic compounds pertinent to urban
929   environments onto mineral dust particles, J. Geophys. Res. Atmos., 109(D2), n/a–n/a, doi:10.1029/2003JD003919,
930   2004.

931 Fang, T., Guo, H., Verma, V., Peltier, R. E. and Weber, R. J.: $PM_{2.5}$ water-soluble elements in the southeastern
932 United States: automated analytical method development, spatiotemporal distributions, source apportionment, and
933 implications for heath studies, Atmos. Chem. Phys., 15(20), 11667–11682, doi:10.5194/acp-15-11667-2015, 2015.

934 Forouzanfar, M. H., Alexander, L., Anderson, H. R., Bachman, V. F., Biryukov, S., Brauer, M., Burnett, R., Casey,
935 D., Coates, M. M., Cohen, A., Delwiche, K., Estep, K., Frostad, J. J., KC, A., Kyu, H. H., Moradi-Lakeh, M., Ng,
936 M., Slepak, E. L., Thomas, B. A., Wagner, J., Aasvang, G. M., Abbafati, C., Ozgoren, A. A., Abd-Allah, F., Abera,
937 S. F., Aboyans, V., Abraham, B., Abraham, J. P., Abubakar, I., Abu-Rmeileh, N. M. E., Aburto, T. C., Achoki, T.,
938 Adelekan, A., Adofo, K., Adou, A. K., Adsuar, J. C., Afshin, A., Agardh, E. E., Al Khabouri, M. J., Al Lami, F. H.,
939 Alam, S. S., Alasfoor, D., Albittar, M. I., Alegretti, M. A., Aleman, A. V, Alemu, Z. A., Alfonso-Cristancho, R.,
940 Alhabib, S., Ali, R., Ali, M. K., Alla, F., Allebeck, P., Allen, P. J., Alsharif, U., Alvarez, E., Alvis-Guzman, N.,
941 Amankwaa, A. A., Amare, A. T., Ameh, E. A., Ameli, O., Amini, H., Ammar, W., Anderson, B. O., Antonio, C. A.
942 T., Anwari, P., Cunningham, S. A., Arnlöv, J., Arsenijevic, V. S. A., Artaman, A., Asghar, R. J., Assadi, R., Atkins,
943 L. S., Atkinson, C., Avila, M. A., Awuah, B., Badawi, A., Bahit, M. C., Bakfalouni, T., Balakrishnan, K., Balalla,
944 S., Balu, R. K., Banerjee, A., Barber, R. M., Barker-Collo, S. L., Barquera, S., Barregard, L., Barrero, L. H.,
945 Barrientos-Gutierrez, T., Basto-Abreu, A. C., Basu, A., Basu, S., Basulaiman, M. O., Ruvalcaba, C. B., Beardsley,
946 J., Bedi, N., Bekele, T., Bell, M. L., Benjet, C., Bennett, D. A., et al.: Global, regional, and national comparative risk
947 assessment of 79 behavioural, environmental and occupational, and metabolic risks or clusters of risks in 188
948 countries, 1990–2013: a systematic analysis for the Global Burden of Disease Study 2013, Lancet,
949 doi:10.1016/S0140-6736(15)00128-2, 2015.

950 Fountoukis, C. and Nenes, A.: ISORROPIA II: a computationally efficient thermodynamic equilibrium model for
951 aerosols, Atmos. Chem. Phys., 7(17), 4639–4659, doi:10.5194/acp-7-4639-2007, 2007.

952 Fujii, Y., Iriana, W., Oda, M., Puriwigati, A., Tohno, S., Lestari, P., Mizohata, A. and Huboyo, H. S.: Characteristics
953 of carbonaceous aerosols emitted from peatland fire in Riau, Sumatra, Indonesia, Atmos. Environ., 87, 164–169,
954 doi:10.1016/j.atmosenv.2014.01.037, 2014.

955 Generoso, S., Bréon, F.-M., Balkanski, Y., Boucher, O. and Schulz, M.: Improving the seasonal cycle and
956 interannual variations of biomass burning aerosol sources, Atmos. Chem. Phys., 3(4), 1211–1222, doi:10.5194/acp-
957 3-1211-2003, 2003.

958 Gibson, M. D., Heal, M. R., Bache, D. H., Hursthouse, A. S., Beverland, I. J., Craig, S. E., Clark, C. F., Jackson, M.
959 H., Guernsey, J. R. and Jones, C.: Using mass reconstruction along a four-site transect as a method to interpret
960 PM10 in west-central Scotland,United Kingdom, J. Air Waste Manage. Assoc., 59(12), 1429–1436,
961 doi:10.3155/1047-3289.59.12.1429, 2009.

962 Gibson, M. D., Pierce, J. R., Waugh, D., Kuchta, J. S., Chisholm, L., Duck, T. J., Hopper, J. T., Beauchamp, S.,
963 King, G. H., Franklin, J. E., Leaitch, W. R., Wheeler, A. J., Li, Z., Gagnon, G. A. and Palmer, P. I.: Identifying the
964 sources driving observed PM2.5 temporal variability over Halifax, Nova Scotia, during BORTAS-B, Atmos. Chem.
965 Phys., 13(14), 7199–7213, doi:10.5194/acp-13-7199-2013, 2013a.

966 Gibson, M. D., Heal, M. R., Li, Z., Kuchta, J., King, G. H., Hayes, A. and Lambert, S.: The spatial and seasonal
967 variation of nitrogen dioxide and sulfur dioxide in Cape Breton Highlands National Park, Canada, and the
968 association with lichen abundance, Atmos. Environ., 64(0), 303–311,
969 doi:http://dx.doi.org/10.1016/j.atmosenv.2012.09.068, 2013b.

970 Giordano, M. R., Short, D. Z., Hosseini, S., Lichtenberg, W. and Asa-Awuku, A. A.: Changes in droplet surface
971 tension affect the observed hygroscopicity of photochemically aged biomass burning aerosol, Environ. Sci.
972 Technol., 47(19), 10980–10986, doi:10.1021/es401867j, 2013.

973 Graham, B., Falkovich, A. H., Rudich, Y., Maenhaut, W., Guyon, P. and Andreae, M. O.: Local and regional
974 contributions to the atmospheric aerosol over Tel Aviv, Israel: a case study using elemental, ionic and organic
975 tracers, Atmos. Environ., 38(11), 1593–1604, doi:http://dx.doi.org/10.1016/j.atmosenv.2003.12.015, 2004.

976 Hand, J. and Malm, W. C.: Review of the IMPROVE equation for estimating ambient light extinction coefficients,
977 Colorado State University, Fort Colins., 2006.

978 Hand, J. L., Schichtel, B. A., Pitchford, M., Malm, W. C. and Frank, N. H.: Seasonal composition of remote and
979 urban fine particulate matter in the United States, J. Geophys. Res., 117(D5), D05209, doi:10.1029/2011JD017122,

980   2012.

981   Henning, S., Weingartner, E., Schwikowski, M., Gäggeler, H. W., Gehrig, R., Hinz, K.-P., Trimborn, A., Spengler,
982   B. and Baltensperger, U.: Seasonal variation of water-soluble ions of the aerosol at the high-alpine site Jungfraujoch
983   (3580 m asl), J. Geophys. Res. Atmos., 108(D1), 4030, doi:10.1029/2002JD002439, 2003.

984   Hersey, S. P., Craven, J. S., Metcalf, A. R., Lin, J., Lathem, T., Suski, K. J., Cahill, J. F., Duong, H. T., Sorooshian,
985   A., Jonsson, H. H., Shiraiwa, M., Zuend, A., Nenes, A., Prather, K. A., Flagan, R. C. and Seinfeld, J. H.:
986   Composition and hygroscopicity of the Los Angeles Aerosol: CalNex, J. Geophys. Res. Atmos., 118(7), 3016–3036,
987   doi:10.1002/jgrd.50307, 2013.

988   Holben, B. N., Eck, T. F., Slutsker, I., Tanré, D., Buis, J. P., Setzer, A., Vermote, E., Reagan, J. A., Kaufman, Y. J.,
989   Nakajima, T., Lavenu, F., Jankowiak, I. and Smirnov, A.: AERONET—A federated instrument network and data
990   archive for aerosol characterization, Remote Sens. Environ., 66(1), 1–16, doi:http://dx.doi.org/10.1016/S0034-
991   4257(98)00031-5, 1998.

992   Huang, J. P., Liu, J. J., Chen, B. and Nasiri, S. L.: Detection of anthropogenic dust using CALIPSO lidar
993   measurements, Atmos. Chem. Phys., 15(20), 11653–11665, doi:10.5194/acp-15-11653-2015, 2015.

994   IMPROVE: Reconstructing Light Extinction from Aerosol Measurements, Reconstr. Light Extinction from Aerosol
995   Meas. Interag. Monit. Prot. Vis. Environ. [online] Available from:
996   http://views.cira.colostate.edu/fed/DataWizard/Default.aspx (Accessed 20 May 2012), 2015.

997   IPCC: Climate Change 2013: The Physical Science Basis. Contribution of Working Group I to the Fifth Assessment
998   Report of the Intergovernmental Panel on Climate Change, 5th ed., edited by T. F. Stocker, D. Qin, G.-K. Plattner,
999   M. Tignor, S. K. Allen, J. Boschung, A. Nauels, Y. Xia, V. Bex, and P. M. Midgley, Cambridge University Press,
1000   Cambridge, United Kingdom and New York, NY, USA., 2013.

1001   Jasan, R. C., Plá, R. R., Invernizzi, R. and Dos Santos, M.: Characterization of atmospheric aerosol in Buenos Aires,
1002   Argentina, J. Radioanal. Nucl. Chem., 281(1), 101–105, doi:10.1007/s10967-009-0071-1, 2009.

1003   Jimenez, J. L., Canagaratna, M. R., Donahue, N. M., Prevot, A. S. H., Zhang, Q., Kroll, J. H., DeCarlo, P. F., Allan,
1004   J. D., Coe, H., Ng, N. L., Aiken, A. C., Docherty, K. S., Ulbrich, I. M., Grieshop, A. P., Robinson, A. L., Duplissy,
1005   J., Smith, J. D., Wilson, K. R., Lanz, V. A., Hueglin, C., Sun, Y. L., Tian, J., Laaksonen, A., Raatikainen, T.,
1006   Rautiainen, J., Vaattovaara, P., Ehn, M., Kulmala, M., Tomlinson, J. M., Collins, D. R., Cubison, M. J., E., Dunlea,
1007   J., Huffman, J. A., Onasch, T. B., Alfarra, M. R., Williams, P. I., Bower, K., Kondo, Y., Schneider, J., Drewnick, F.,
1008   Borrmann, S., Weimer, S., Demerjian, K., Salcedo, D., Cottrell, L., Griffin, R., Takami, A., Miyoshi, T.,
1009   Hatakeyama, S., Shimono, A., Sun, J. Y., Zhang, Y. M., Dzepina, K., Kimmel, J. R., Sueper, D., Jayne, J. T.,
1010   Herndon, S. C., Trimborn, A. M., Williams, L. R., Wood, E. C., Middlebrook, A. M., Kolb, C. E., Baltensperger, U.
1011   and Worsnop, D. R.: Evolution of organic aerosols in the atmosphere, Science, 326(5959), 1525–1529,
1012   doi:10.1126/science.1180353, 2009.

1013   Kahn, R. A. and Gaitley, B. J.: An analysis of global aerosol type as retrieved by MISR, J. Geophys. Res. Atmos.,
1014   120(9), 4248–4281, doi:10.1002/2015JD023322, 2015.

1015   Kloog, I., Koutrakis, P., Coull, B. A., Lee, H. J. and Schwartz, J.: Assessing temporally and spatially resolved
1016   PM2.5 exposures for epidemiological studies using satellite aerosol optical depth measurements, Atmos. Environ.,
1017   45(35), 6267–6275, doi:10.1016/j.atmosenv.2011.08.066, 2011.

1018   Kloog, I., Ridgway, B., Koutrakis, P., Coull, B. A. and Schwartz, J. D.: Long- and short-term exposure to PM(2.5)
1019   and mortality: Using novel exposure models, Epidemiology, 24(4), 555–561, doi:10.1097/EDE.0b013e318294beaa,
1020   2013.

1021   Koepke, P., Hess, M., Schult, I. and Shettle, E. P.: Global Aerosol Dataset, Report N 243, Hamburg., 1997.

1022   Kreidenweis, S. M., Petters, M. D. and DeMott, P. J.: Single-parameter estimates of aerosol water content, Environ.
1023   Res. Lett., 3(3), 35002, doi:10.1088/1748-9326/3/3/035002, 2008.

1024   Laden, F., Schwartz, J., Speizer, F. E. and Dockery, D. W.: Reduction in fine particulate air pollution and mortality,
1025   Am. J. Respir. Crit. Care Med., 173(6), 667–672, doi:10.1164/rccm.200503-443OC, 2006.

1026   Latham, J., Cumani, R., Rosati, I. and Bloise, M.: Global Land Cover SHARE (GLC-SHARE) database Beta-

1027   Release Version 1.0-2014, Rome., 2014.

1028   Lathem, T. L., Beyersdorf, A. J., Thornhill, K. L., Winstead, E. L., Cubison, M. J., Hecobian, A., Jimenez, J. L.,
1029   Weber, R. J., Anderson, B. E. and Nenes, A.: Analysis of CCN activity of Arctic aerosol and Canadian biomass
1030   burning during summer 2008, Atmos. Chem. Phys., 13(5), 2735–2756, doi:10.5194/acp-13-2735-2013, 2013.

1031   Lee, H. J., Coull, B. A., Bell, M. L. and Koutrakis, P.: Use of satellite-based aerosol optical depth and spatial
1032   clustering to predict ambient PM2.5 concentrations., Environ. Res., 118, 8–15, doi:10.1016/j.envres.2012.06.011,
1033   2012.

1034   Lelieveld, J., Evans, J. S., Fnais, M., Giannadaki, D. and Pozzer, A.: The contribution of outdoor air pollution
1035   sources to premature mortality on a global scale, Nature, 525(7569), 367–371, 2015.

1036   Lepeule, J., Laden, F., Dockery, D. and Schwartz, J.: Chronic Exposure to Fine Particles and Mortality: An
1037   Extended Follow-up of the Harvard Six Cities Study from 1974 to 2009, Environ. Health Perspect., 120(7), 965–
1038   970, doi:10.1289/ehp.1104660, 2012.

1039   Lestari, P. and Mauliadi, Y. D.: Source apportionment of particulate matter at urban mixed site in Indonesia using
1040   PMF, Atmos. Environ., 43(10), 1760–1770, doi:http://dx.doi.org/10.1016/j.atmosenv.2008.12.044, 2009.

1041   Lin, C., Li, Y., Yuan, Z., Lau, A. K. H., Li, C. and Fung, J. C. H.: Using satellite remote sensing data to estimate the
1042   high-resolution distribution of ground-level PM2.5, Remote Sens. Environ., 156, 117–128,
1043   doi:10.1016/j.rse.2014.09.015, 2015.

1044   Lippmann, M.: Toxicological and epidemiological studies of cardiovascular effects of ambient air fine particulate
1045   matter (PM2.5) and its chemical components: Coherence and public health implications, Crit. Rev. Toxicol., 44(4),
1046   299–347, doi:10.3109/10408444.2013.861796, 2014.

1047   Liu, Y., Monod, A., Tritscher, T., Praplan, A. P., DeCarlo, P. F., Temime-Roussel, B., Quivet, E., Marchand, N.,
1048   Dommen, J. and Baltensperger, U.: Aqueous phase processing of secondary organic aerosol from isoprene
1049   photooxidation, Atmos. Chem. Phys., 12(13), 5879–5895, doi:10.5194/acp-12-5879-2012, 2012.

1050   Malm, W. C., Sisler, J. F., Huffman, D., Eldred, R. A. and Cahill, T. A.: Spatial and seasonal trends in particle
1051   concentration and optical extinction in the United States, J. Geophys. Res., 99(D1), 1347–1370, 1994.

1052   Misra, A., Gaur, A., Bhattu, D., Ghosh, S., Dwivedi, A. K., Dalai, R., Paul, D., Gupta, T., Tare, V., Mishra, S. K.,
1053   Singh, S. and Tripathi, S. N.: An overview of the physico-chemical characteristics of dust at Kanpur in the central
1054   Indo-Gangetic basin, Atmos. Environ., 97, 386–396, doi:10.1016/j.atmosenv.2014.08.043, 2014.

1055   Munchak, L. A., Schichtel, B. A., Sullivan, A. P., Holden, A. S., Kreidenweis, S. M., Malm, W. C. and Collett, J. L.:
1056   Development of wildland fire particulate smoke marker to organic carbon emission ratios for the conterminous
1057   United States, Atmos. Environ., 45(2), 395–403, doi:10.1016/j.atmosenv.2010.10.006, 2011.

1058   Oanh, N. T. K., Upadhyay, N., Zhuang, Y.-H., Hao, Z.-P., Murthy, D. V. S., Lestari, P., Villarin, J. T., Chengchua,
1059   K., Co, H. X., Dung, N. T. and Lindgren, E. S.: Particulate air pollution in six Asian cities: Spatial and temporal
1060   distributions, and associated sources, Atmos. Environ., 40(18), 3367–3380,
1061   doi:http://dx.doi.org/10.1016/j.atmosenv.2006.01.050, 2006.

1062   Padró, L. T., Moore, R. H., Zhang, X., Rastogi, N., Weber, R. J. and Nenes, A.: Mixing state and compositional
1063   effects on CCN activity and droplet growth kinetics of size-resolved CCN in an urban environment, Atmos. Chem.
1064   Phys., 12(21), 10239–10255, doi:10.5194/acp-12-10239-2012, 2012.

1065   Patadia, F., Kahn, R. A., Limbacher, J. A., Burton, S. P., Ferrare, R. A., Hostetler, C. A. and Hair, J. W.: Aerosol
1066   airmass type mapping over the Urban Mexico City region from space-based multi-angle imaging, Atmos. Chem.
1067   Phys., 13(18), 9525–9541, doi:10.5194/acp-13-9525-2013, 2013.

1068   Petters, M. D. and Kreidenweis, S. M.: A single parameter representation of hygroscopic growth and cloud
1069   condensation nucleus activity, Atmos. Chem. Phys., 7(8), 1961–1971, doi:10.5194/acp-7-1961-2007, 2007.

1070   Petters, M. D. and Kreidenweis, S. M.: A single parameter representation of hygroscopic growth and cloud
1071   condensation nucleus activity – Part 2: Including solubility, Atmos. Chem. Phys., 8(20), 6273–6279,
1072   doi:10.5194/acp-8-6273-2008, 2008.

1073   Petters, M. D. and Kreidenweis, S. M.: A single parameter representation of hygroscopic growth and cloud
1074   condensation nucleus activity; Part 3: Including surfactant partitioning, Atmos. Chem. Phys., 13(2), 1081–1091,
1075   doi:10.5194/acp-13-1081-2013, 2013.

1076   Petzold, A., Ogren, J. A., Fiebig, M., Laj, P., Li, S.-M., Baltensperger, U., Holzer-Popp, T., Kinne, S., Pappalardo,
1077   G., Sugimoto, N., Wehrli, C., Wiedensohler, A. and Zhang, X.-Y.: Recommendations for reporting "black carbon"
1078   measurements, Atmos. Chem. Phys., 13(16), 8365–8379, doi:10.5194/acp-13-8365-2013, 2013.

1079   Philip, S., Martin, R. V, van Donkelaar, A., Lo, J. W.-H., Wang, Y., Chen, D., Zhang, L., Kasibhatla, P. S., Wang,
1080   S., Zhang, Q., Lu, Z., Streets, D. G., Bittman, S. and Macdonald, D. J.: Global chemical composition of ambient fine
1081   particulate matter for exposure assessment, Environ. Sci. Technol., 48(22), 13060–13068, doi:10.1021/es502965b,
1082   2014a.

1083   Philip, S., Martin, R. V., Pierce, J. R., Jimenez, J. L., Zhang, Q., Canagaratna, M. R., Spracklen, D. V., Nowlan, C.
1084   R., Lamsal, L. N., Cooper, M. J. and Krotkov, N. A.: Spatially and seasonally resolved estimate of the ratio of
1085   organic mass to organic carbon, Atmos. Environ., 87, 34–40, doi:10.1016/j.atmosenv.2013.11.065, 2014b.

1086   Pitchford, M., Malm, W., Schichtel, B., Kumar, N., Lowenthal, D. and Hand, J.: Revised algorithm for estimating
1087   light extinction from IMPROVE particle speciation data, J. Air Waste Manage. Assoc., 57(11), 1326–1336,
1088   doi:10.3155/1047-3289.57.11.1326, 2007.

1089   Prenni, A. J., Petters, M. D., Kreidenweis, S. M., DeMott, P. J. and Ziemann, P. J.: Cloud droplet activation of
1090   secondary organic aerosol, J. Geophys. Res., 112(D10), D10223, doi:10.1029/2006JD007963, 2007.

1091   Putaud, J.-P., Raes, F., Van Dingenen, R., Brüggemann, E., Facchini, M.-C., Decesari, S., Fuzzi, S., Gehrig, R.,
1092   Hüglin, C., Laj, P., Lorbeer, G., Maenhaut, W., Mihalopoulos, N., Müller, K., Querol, X., Rodriguez, S., Schneider,
1093   J., Spindler, G., Brink, H. ten, Tørseth, K. and Wiedensohler, A.: A European aerosol phenomenology—2: chemical
1094   characteristics of particulate matter at kerbside, urban, rural and background sites in Europe, Atmos. Environ.,
1095   38(16), 2579–2595, doi:http://dx.doi.org/10.1016/j.atmosenv.2004.01.041, 2004.

1096   Putaud, J.-P., Van Dingenen, R., Alastuey, A., Bauer, H., Birmili, W., Cyrys, J., Flentje, H., Fuzzi, S., Gehrig, R.,
1097   Hansson, H. C., Harrison, R. M., Herrmann, H., Hitzenberger, R., Hüglin, C., Jones, A. M., Kasper-Giebl, A., Kiss,
1098   G., Kousa, A., Kuhlbusch, T. A. J., Löschau, G., Maenhaut, W., Molnar, A., Moreno, T., Pekkanen, J., Perrino, C.,
1099   Pitz, M., Puxbaum, H., Querol, X., Rodriguez, S., Salma, I., Schwarz, J., Smolik, J., Schneider, J., Spindler, G., ten
1100   Brink, H., Tursic, J., Viana, M., Wiedensohler, A. and Raes, F.: A European aerosol phenomenology – 3: Physical
1101   and chemical characteristics of particulate matter from 60 rural, urban, and kerbside sites across Europe, Atmos.
1102   Environ., 44(10), 1308–1320, doi:10.1016/j.atmosenv.2009.12.011, 2010.

1103   Quincey, P., Butterfield, D., Green, D., Coyle, M. and Cape, J. N.: An evaluation of measurement methods for
1104   organic, elemental and black carbon in ambient air monitoring sites, Atmos. Environ., 43(32), 5085–5091,
1105   doi:http://dx.doi.org/10.1016/j.atmosenv.2009.06.041, 2009.

1106   Ram, K., Sarin, M. M. and Tripathi, S. N.: Temporal trends in atmospheric PM2.5, PM10, elemental carbon, organic
1107   carbon, water-soluble organic carbon, and optical properties: Impact of biomass burning emissions in the Indo-
1108   Gangetic Plain, Environ. Sci. Technol., 46(2), 686–695, doi:10.1021/es202857w, 2012.

1109   Remoundaki, E., Kassomenos, P., Mantas, E., Mihalopoulos, N. and Tsezos, M.: Composition and mass closure of
1110   PM2.5 in urban environment (Athens, Greece), Aerosol Air Qual. Res., 13(1), 72–82, 2013.

1111   Rice, E. W., Bridgewater, L., Association, A. P. H., Association, A. W. W. and Federation, W. E.: Standard
1112   Methods for the Examination of Water and Wastewater, American Public Health Association., 2012.

1113   Rickards, A. M. J., Miles, R. E. H., Davies, J. F., Marshall, F. H. and Reid, J. P.: Measurements of the sensitivity of
1114   aerosol hygroscopicity and the κ parameter to the O/C ratio, J. Phys. Chem. A, 117(51), 14120–14131,
1115   doi:10.1021/jp407991n, 2013.

1116   Robinson, C. B., Schill, G. P., Zarzana, K. J. and Tolbert, M. A.: Impact of organic coating on optical growth of
1117   ammonium sulfate particles, Environ. Sci. Technol., 47(23), 13339–13346, doi:10.1021/es4023128, 2013.

1118   Santoso, M., Dwiana Lestiani, D. and Hopke, P. K.: Atmospheric black carbon in PM2.5 in Indonesian cities, J. Air
1119   Waste Manage. Assoc., 63(9), 1022–1025, doi:10.1080/10962247.2013.804465, 2013.

1120 Snider, G., Weagle, C. L., Martin, R. V., van Donkelaar, A., Conrad, K., Cunningham, D., Gordon, C., Zwicker, M.,
1121 Akoshile, C., Artaxo, P., Anh, N. X., Brook, J., Dong, J., Garland, R. M., Greenwald, R., Griffith, D., He, K.,
1122 Holben, B. N., Kahn, R., Koren, I., Lagrosas, N., Lestari, P., Ma, Z., Vanderlei Martins, J., Quel, E. J., Rudich, Y.,
1123 Salam, A., Tripathi, S. N., Yu, C., Zhang, Q., Zhang, Y., Brauer, M., Cohen, A., Gibson, M. D. and Liu, Y.:
1124 SPARTAN: a global network to evaluate and enhance satellite-based estimates of ground-level particulate matter for
1125 global health applications, Atmos. Meas. Tech., 8(1), 505–521, doi:10.5194/amt-8-505-2015, 2015.

1126 Sorooshian, A., Hersey, S., Brechtel, F. J., Corless, A., Flagan, R. C. and Seinfeld, J. H.: Rapid, size-resolved
1127 aerosol hygroscopic growth measurements: differential aerosol sizing and hygroscopicity spectrometer probe
1128 (DASH-SP), Aerosol Sci. Technol., 42(6), 445–464, doi:10.1080/02786820802178506, 2008.

1129 Sun, Y.-L., Zhang, Q., Schwab, J. J., Demerjian, K. L., Chen, W.-N., Bae, M.-S., Hung, H.-M., Hogrefe, O., Frank,
1130 B., Rattigan, O. V. and Lin, Y.-C.: Characterization of the sources and processes of organic and inorganic aerosols
1131 in New York city with a high-resolution time-of-flight aerosol mass apectrometer, Atmos. Chem. Phys., 11(4),
1132 1581–1602, doi:10.5194/acp-11-1581-2011, 2011.

1133 Svenningsson, B., Rissler, J., Swietlicki, E., Mircea, M., Bilde, M., Facchini, M. C., Decesari, S., Fuzzi, S., Zhou, J.,
1134 Mønster, J. and Rosenørn, T.: Hygroscopic growth and critical supersaturations for mixed aerosol particles of
1135 inorganic and organic compounds of atmospheric relevance, Atmos. Chem. Phys., 6(7), 1937–1952,
1136 doi:10.5194/acp-6-1937-2006, 2006.

1137 Swietlicki, E., Hansson, H.-C., Hämeri, K., Svenningsson, B., Massling, A., McFiggans, G., McMurry, P. H., Petäjä,
1138 T., Tunved, P., Gysel, M., Topping, D., Weingartner, E., Baltensperger, U., Rissler, J., Wiedensohler, A. and
1139 Kulmala, M.: Hygroscopic properties of submicrometer atmospheric aerosol particles measured with H-TDMA
1140 instruments in various environments—a review, Tellus B, 60(3), 432–469, 2008.

1141 Taha, G., Box, G. P., Cohen, D. D. and Stelcer, E.: Black carbon measurement using laser integrating plate method,
1142 Aerosol Sci. Technol., 41(3), 266–276, doi:10.1080/02786820601156224, 2007.

1143 USEPA: Chemical Speciation Network Database, [online] Available from:
1144 http://views.cira.colostate.edu/fed/DataWizard/Default.aspx (Accessed 1 December 2015), 2015.

1145 van Donkelaar, A., Martin, R. V, Brauer, M. and Boys, B. L.: Use of satellite observations for long-term exposure
1146 assessment of global concentrations of fine particulate matter, Environ. Health Perspect., 123(2), 135–143,
1147 doi:10.1289/ehp.1408646, 2015.

1148 Varutbangkul, V., Brechtel, F. J., Bahreini, R., Ng, N. L., Keywood, M. D., Kroll, J. H., Flagan, R. C., Seinfeld, J.
1149 H., Lee, A. and Goldstein, A. H.: Hygroscopicity of secondary organic aerosols formed by oxidation of
1150 cycloalkenes, monoterpenes, sesquiterpenes, and related compounds, Atmos. Chem. Phys., 6(9), 2367–2388,
1151 doi:10.5194/acp-6-2367-2006, 2006.

1152 Villalobos, A. M., Amonov, M. O., Shafer, M. M., Devi, J. J., Gupta, T., Tripathi, S. N., Rana, K. S., Mckenzie, M.,
1153 Bergin, M. H. and Schauer, J. J.: Source apportionment of carbonaceous fine particulate matter (PM2.5) in two
1154 contrasting cities across the Indo–Gangetic Plain, Atmos. Pollut. Res., 6(3), 398, 2015.

1155 Vu Van, H., Le Xuan, Q., Pham Ngoc, H. and Luc, H.: Health risk assessment of mobility-related air pollution in Ha
1156 Noi, Vietnam, J. Environ. Prot. (Irvine,. Calif)., 4(10), 1165–1172, 2013.

1157 Wagner, F., Bortoli, D., Pereira, S., João Costa, M., Silva, A. M., Weinzierl, B., Esselborn, M., Petzold, A., Rasp,
1158 K., Heinold, B. and Tegen, I.: Properties of dust aerosol particles transported to Portugal from the Sahara desert,
1159 Tellus B, 61(1), 297–306, 2009.

1160 Wang, J. L.: Mapping the global dust storm records: Review of dust data sources in supporting modeling/climate
1161 study, Curr. Pollut. Reports, 1(2), 82–94, doi:10.1007/s40726-015-0008-y, 2015.

1162 Wang, Z., Chen, L., Tao, J., Zhang, Y. and Su, L.: Satellite-based estimation of regional particulate matter (PM) in
1163 Beijing using vertical-and-RH correcting method, Remote Sens. Environ., 114(1), 50–63,
1164 doi:http://dx.doi.org/10.1016/j.rse.2009.08.009, 2010.

1165 Wexler, A. S. and Clegg, S. L.: Atmospheric aerosol models for systems including the ions H+, NH4+, Na+, SO42−,
1166 NO3−, Cl−, Br−, and H2O, J. Geophys. Res. Atmos., 107(D14), ACH14–1–14, doi:10.1029/2001JD000451, 2002.

1167 WHO: Human exposure to air pollution, in Update of the World Air Quality Guidelines World Health Organization,
1168 pp. 61–86, World Health Organization, Geneva, Switzerland., 2005.

1169 WHO: WHO | Air quality guidelines - global update 2005, World Health Organization, Geneva, Switzerland., 2006.

1170 Wise, M. E., Surratt, J. D., Curtis, D. B., Shilling, J. E. and Tolbert, M. A.: Hygroscopic growth of ammonium
1171 sulfate/dicarboxylic acids, J. Geophys. Res. Atmos., 108(D20), 4638, doi:10.1029/2003JD003775, 2003.

1172 Yang, F., Tan, J., Zhao, Q., Du, Z., He, K., Ma, Y., Duan, F. and Chen, G.: Characteristics of $PM_{2.5}$ speciation in
1173 representative megacities and across China, Atmos. Chem. Phys., 11(11), 5207–5219, doi:10.5194/acp-11-5207-
1174 2011, 2011.

1175 Zhang, R., Jing, J., Tao, J., Hsu, S.-C., Wang, G., Cao, J., Lee, C. S. L., Zhu, L., Chen, Z., Zhao, Y. and Shen, Z.:
1176 Chemical characterization and source apportionment of $PM_{2.5}$ in Beijing: seasonal perspective, Atmos. Chem. Phys.,
1177 13(14), 7053–7074, doi:10.5194/acp-13-7053-2013, 2013.

1178 Zhang, W.-J., Sun, Y.-L., Zhuang, G.-S. and Xu, D.-Q.: Characteristics and seasonal variations of PM2.5, PM10,
1179 and TSP aerosol in Beijing, Biomed. Environ. Sci., 19(6), 461–468, 2006.

1180

1181

Figures and Tables

Table 1: Summary of speciation definitions

Species (at 0% RH)	Measurement Method	Species Mass (µg). For concentrations, divide masses by sampling volume v	Reference
SS	IC (anion and cation)	$2.54[Na^+]_{SS}$, where $[Na^+]_{SS} = [Na^+]_{tot} - 0.1[Al]$	(Remoundaki et al., 2013) (Malm et al., 1994)
ANO$_3$		$1.29[NO_3^-]$	(Malm et al., 1994)
ASO$_4$		$[SO_4^{2-}]_{non-ss} + [NH_4^+] - 0.29[NO_3^-]$, where $[SO_4^{2-}]_{non-ss} = [SO_4^{2-}]_{total} - 0.12[Na^+]$	(Dabek-Zlotorzynska et al., 2011; Henning et al., 2003)
Na$_2$SO$_4$		$0.18[Na^+]_{SS}$	
CM	ICP-MS	$10\times([Al] + [Mg] + [Fe])$	(Wang, 2015)
EBC	SSR	$20.7 \times \ln(R_o/R)$	(Taha et al., 2007)
TEO	ICP-MS	$1.47[V] + 1.27[Ni] +1.25[Cu] + 1.24[Zn] + 1.32[As] + 1.2[Se] + 1.07[Ag] + 1.14[Cd] + 1.2[Sb] + 1.12[Ba] + 1.23[Ce] +1.08[Pb]$	(Malm et al., 1994)
PBW$_{inorg}$	$\kappa_{m,X}$	$\sum_X [f_{m,X}(RH) - 1][X]$	(Kreidenweis et al., 2008)
PBW$_{RM}$		$RM(1 - 1/f_{m,RM})$	Table 2
RM(35%)	Mass Balance	$[PM_{2.5}] - \{[EBC] + [CM] + [TEO] + [ANO_3] + [SS] + [ASO_4] + [Na_2SO_4] + [PBW]_{inorg}\}$	This Study
RM(0%)	Mass Balance $\kappa_{m,OM} = 0.07$	$RM(35\%) - PBW_{RM}$	Organic growth factors: (Jimenez et al., 2009; Sun et al., 2011)

Species: EBC = Equivalent black carbon, TEO = Trace metal oxides, CM = Crustal Material, ANO$_3$ = Ammonium nitrate, ASO$_4$ = Ammoniated sulfate, PBW = particle-bound water, RM = residual matter (assumed representative of organic matter), [X] = concentration of any hygroscopic species. **Measurement Instruments:** IC = Ion Chromatography, ICP-MS Inductively coupled plasma mass spectrometry, SSR = Smoke Stain Reflectometer, $\kappa_{m,X}$ = single-parameter hygroscopicity by mass (Kreidenweis et al., 2008). RH = Relative Humidity,

Table 2: κ-Kohler constants for volume (κ$_v$), mass (κ$_m$), and related quantities

Compound [X]	$\kappa_{v,X}$	Approximate Density (ρ_X/ρ_{water})	$\kappa_{m,X}$	PBW(%mass) at RH = 35%	RH = 80%
Crustal	0	2.5[a]	0	0	0
EBC	0	1.8[b]	0	0	0
TEO	0	2.5	0	0	0
RM	0.1[c]	1.4	0.07	2	12
ANO$_3$	0.41	1.72	0.24	17	61
ASO$_4$	0.51	1.76	0.29	15	56
Na$_2$SO$_4$	0.68[d]	2.68[d]	0.25	12	50
SS	1.5[e]	2.16	0.69	22	68

PBW = Particle-bound water. EBC = Equivalent black carbon, TEO = Trace Element Oxides, RM = Residual Matter (associated with organics), ANO$_3$ = ammonium nitrate, ASO$_4$ = Ammoniated sulfate. [a] Wagner et al. (2009), [b] Bond and Bergstrom (2006), [c] Assuming an urban O:C ratio of 0.5 then $\kappa_{v,OM} = 0.1$ Jimenez et al. (2009), [d] Petters and Kreidenweis (2007). [e] Fitted using non-deliquesced, subsaturated AIM Model III values, plus 0% RH endpoint by Kreidenweis et al. (2008).

Table 3: PM$_{2.5}$ composition and water content (µg m^{-3}) at each SPARTAN location.

City	Host Institute	Lat/Lon (°)	Elev./Inst. Elev. (m)	Filters (n)	ASO$_4$	ANO$_3$	CM	SS	EBC	TEO	RM	PBW 35%RH	ρ 0%RH (g/cm^3)	NO$_3$ vs. NH$_4^+$ (r^2)	PM$_{2.5}$	PM$_{2.5}$/PM$_{10}$	κ$_{v,tot}$	PM$_{2.5}$ K/Al	PM$_{2.5}$ Zn/Al	Filter Sampling Period
Beijing	Tsinghua University	40.010, 116.333	60// 7.5	114	12.0[a] (7.9)	5.5 (6.4)	15.9 (8.8)	1.5 (2.1)	5.7 (3.4)	0.62 (0.51)	23.8 (18)	4.7 (2.8)	1.69	0.32	69.5 (2.5)	0.49	0.19	2.9	0.51	2013/06 –2016/02
Bandung	ITB Bandung	-6.888, 107.610	826// 20	77	6.0 (2.3)	0.7 (1.3)	2.5 (1.5)	0.3 (0.2)	3.7 (2.0)	0.14 (0.11)	16.0 (5.9)	1.9 (0.6)	1.55	0.06	31.4 (1.0)	0.58	0.17	6.8	0.52	2014/01 –2015/11
Manila	Manila Observatory	14.635, 121.080	60// 10	63	2.7 (1.5)	0.3 (0.2)	1.9 (1.0)	0.5 (0.4)	4.3 (3.3)	0.13 (0.13)	7.3 (3.5)	1.1 (0.5)	1.61	0.03	18.2 (0.8)	0.39	0.16	6.3	1.03	2014/02 – 2016/01
Dhaka	Dhaka University	23.728, 90.398	20// 20	41	7.5 (4.3)	2.1 (1.8)	5.9 (4.0)	1.4 (1.7)	8.4 (5.1)	1.50 (1.46)	21.4 (16)	3.5 (2.2)	1.63	0.43	51.9 (3.7)	0.40	0.17	5.3	3.39	2014/05 –2015/11
Ilorin	Ilorin University	8.484, 4.675	330// 10	40	1.9 (0.8)	0.3 (0.1)	3.0 (2.2)	0.3 (0.4)	1.6 (0.8)	0.09 (0.07)	7.6 (3.8)	0.9 (0.4)	1.62	0.05	15.7 (0.8)	0.44	0.15	2.9	0.49	2014/03 – 2015/10
Kanpur	IIT Kanpur	26.519, 80.233	130// 10	33	17.6 (12)	6.8 (5.3)	4.4 (2.3)	0.6 (0.3)	8.3 (4.7)	0.47 (0.36)	54.6 (33)	6.3 (3.6)	1.52	0.58	99.3 (9.1)	0.56	0.18	16.2	1.01	2013/12 – 2014/11
Buenos Aires	CITEDEF	-34.560, -58.506	25// 7	31	1.1 (0.5)	0.8 (0.4)	2.2 (1.6)	0.6 (0.3)	1.7 (1.2)	0.12 (0.12)	3.1 (1.8)	0.9 (0.3)	1.70	0.28	10.1 (0.6)	0.39	0.19	2.7	0.44	2014/10 – 2016/02
Rehovot	Weizmann Institute	31.907, 34.810	20// 10	30	4.7 (1.9)	0.9 (0.5)	3.3 (1.6)	0.7 (0.6)	2.2 (2.0)	0.12 (0.13)	2.6 (2.8)	1.6 (0.6)	1.79	0.01	16.1 (1.0)	0.40	0.28	2.7	0.40	2015/02 –2016/02
Mammoth Cave NP	Mammoth Cave	37.132, -86.148	235// 7	19	4.1 (2.4)	0.2 (0.1)	1.4 (1.4)	0.1 (0.1)	0.7 (0.4)	0.02 (0.03)	6.1 (4.3)	1.0 (0.5)	1.59	0.00	13.6 (1.8)	0.56	0.22	1.1	0.13	2014/04- 2014/08
Atlanta	Emory University	33.688, -84.290	250// 2	13	2.0 (0.9)	0.3 (0.1)	1.0 (0.4)	0.1 (0.1)	1.1 (1.0)	0.04 (0.02)	4.1 (1.8)	0.6 (0.2)	1.61	0.00	9.1 (0.7)	0.69	0.17	1.9	0.26	2014/01 –2014/05
Singapore	NUS	1.298, 103.780	10// 20	12	16.1 (6.5)	1.2 (0.9)	0.8 (0.3)	0.9 (0.4)	3.1 (2.7)	0.20 (0.16)	39.8 (29)	5.0 (2.4)	1.48	0.66	66.8 (11)	NA	0.21	13.2	1.53	2015/08 – 2015/12
Hanoi	Vietnam Acad. Sci.	21.048, 105.800	10// 20	10	6.0 (2.1)	1.6 (0.4)	5.6 (5.4)	0.9 (0.2)	3.7 (2.1)	0.69 (0.43)	18.2 (7.8)	2.6 (0.7)	1.59	0.22	39.4 (3.9)	0.38	0.18	8.9	3.74	2015/05 – 2015/08
Pretoria	CSIR	-25.756, 28.280	1310// 10	5	1.2 (1.6)	0.7 (0.3)	1.3 (1.8)	0.2 (0.1)	1.4 (0.9)	0.04 (0.04)	1.0 (0.7)	0.5 (0.4)	2.09	0.48	6.4 (2.3)	0.32	0.24	6.0	0.86	2015/09- 2015/11
SPARTAN mean (% mass)	All sites			497	20 (11)%	4.7 (3.0)%	13.4 (9.9)%	2.3 (1.6)%	11.9 (8.4)%	1.0 (1.1)%	40 (24)%	7.2 (3.3)%	1.65	0.24	32.4 (2.9)	0.50	0.20	4.6[b]	0.73[b]	2013 – 2016

[a]Values in parentheses are 1σ standard deviations. RH = Relative Humidity, ANO$_3$ = ammonium nitrate, ASO$_4$ = Ammoniated sulfate, CM = Crustal material, EBC = Equivalent black carbon, TEO = Trace Element Oxides, RM = Residual Matter, PBW = Particle-bound water. Mean Na$_2$SO$_4$ was not significant (< 0.1 µg m^{-3}) at any SPARTAN site. [b]Geometric mean
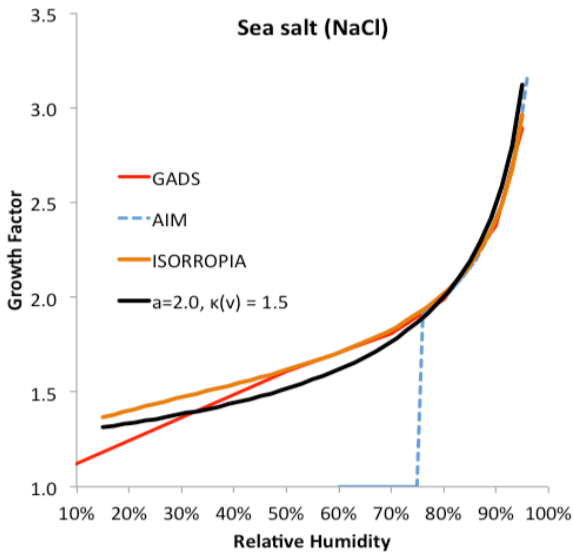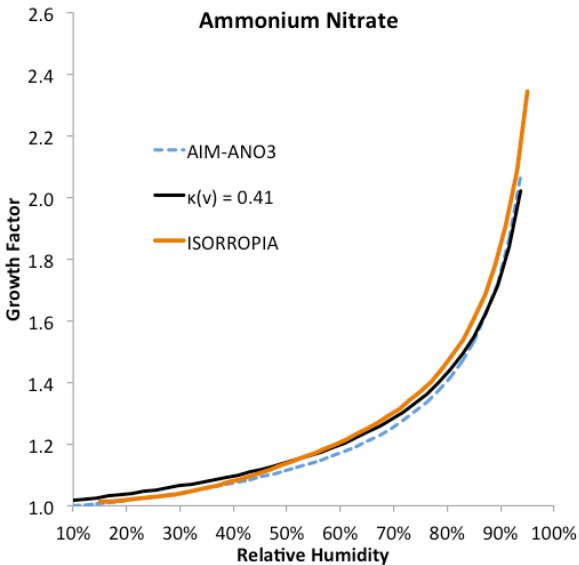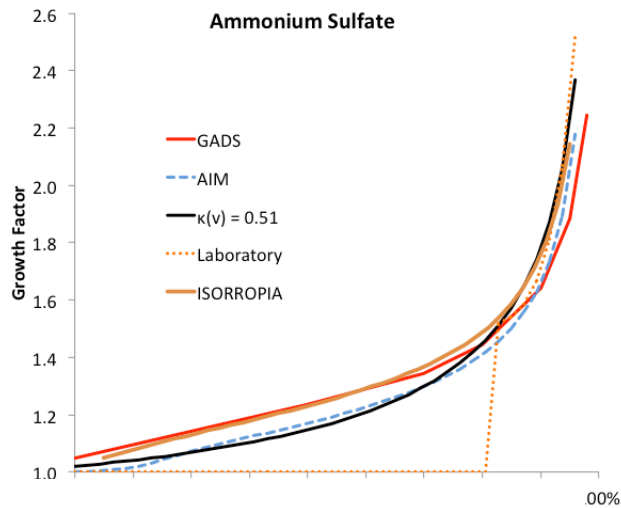
Figure 1: Hygroscopic growth factors for ammonium sulfate (top), ammonium nitrate (centre), and sea salt (bottom). GADS = Global Aerosol Dataset estimated from empirical data (Koepke et al., 1997). ISORROPIA = Aerosol thermodynamic model at T=298K (reverse mode) and assuming linear water/solvent volume additivity (Fountoukis and Nenes, 2007). AIM = Aerosol Inorganic Model calculated metastable growth for ammonium sulfate and ammonium nitrate at T=298K (Wexler and Clegg, 2002), Laboratory ammonium sulfate fit is $GF = 1.49 + 2.81 \cdot RH^{24.6}$ (with deliquescence at 80%) for bulk pure ammonium sulfate (Wise et al., 2003). All components are fit using Eq 6.
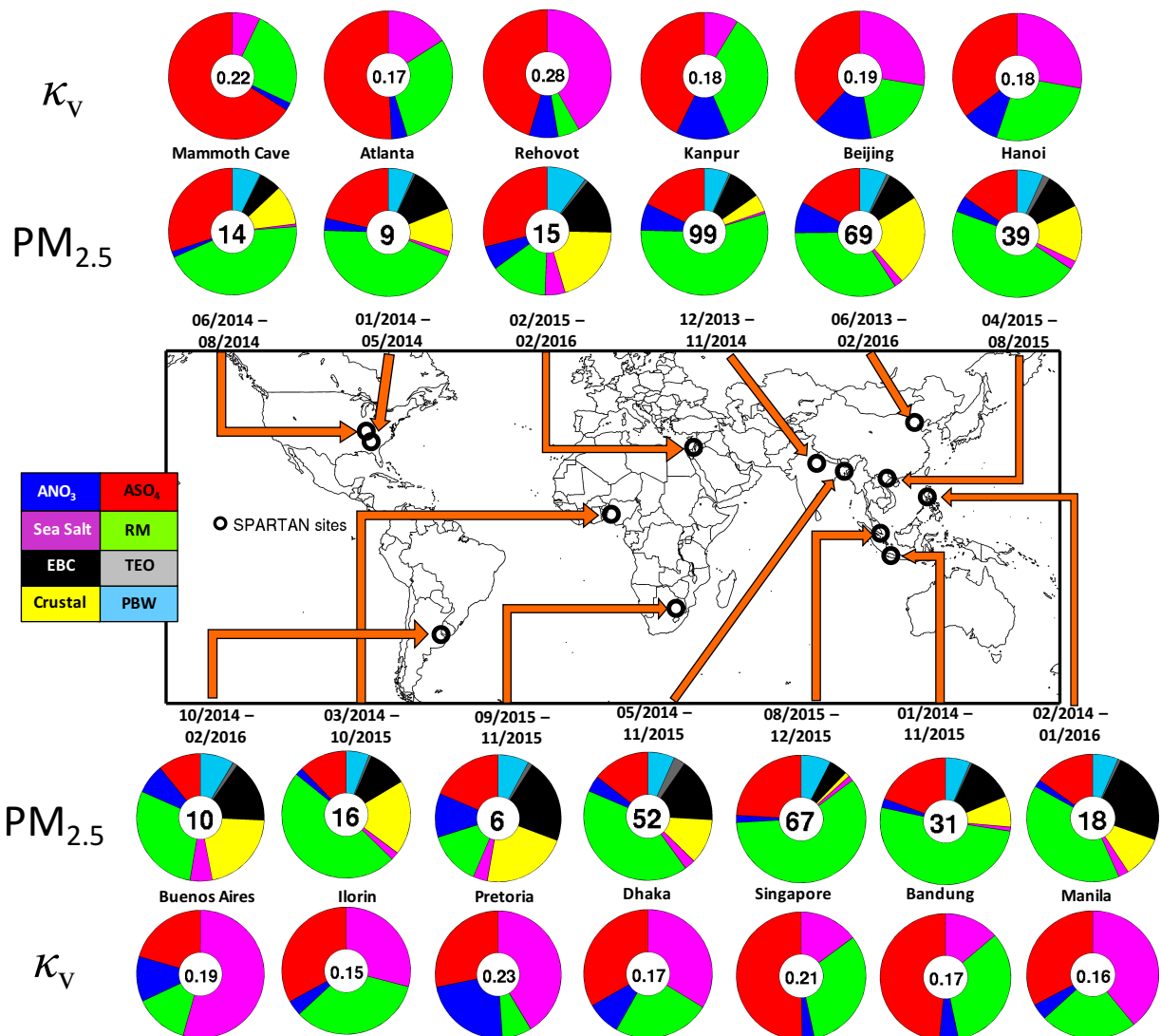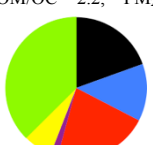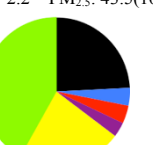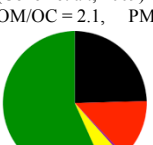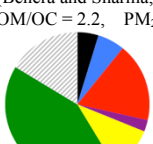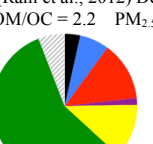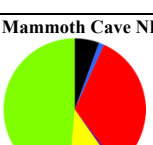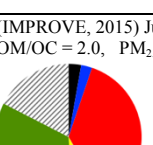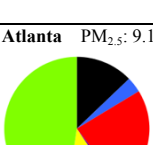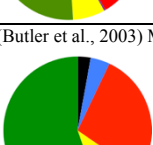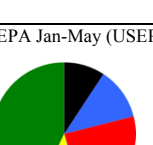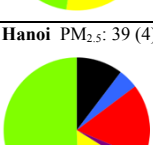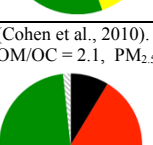
Figure 2: PM$_{2.5}$ mass (inner circle, μg m^{-3}) and composition mass fraction (filled colors) is shown in interior pie charts. Exterior pie charts contain site-mean κ_v surrounded by the relative contribution of PBW water at 35% RH.

Figure 3: Comparison of SPARTAN water-free aerosol composition with 11 collocated speciation studies. The numbers in parentheses show 1-σ deviations of averaged masses. The number of filters sampled is _n_. Dark green = organic, Light green = residual matter, black = equivalent black carbon, red = Ammoniated sulfate, blue = ammonium nitrate, purple = sea salt, yellow = crustal, and grey stripes = unknown. OM/OC ratios are from Philip et al. (2014b) and Canagaratna et al. (2015). Relative mass percentages are based on water-free aerosol components. SPARTAN percentages are renormalized to 100% after omission of species not found in comparison studies.

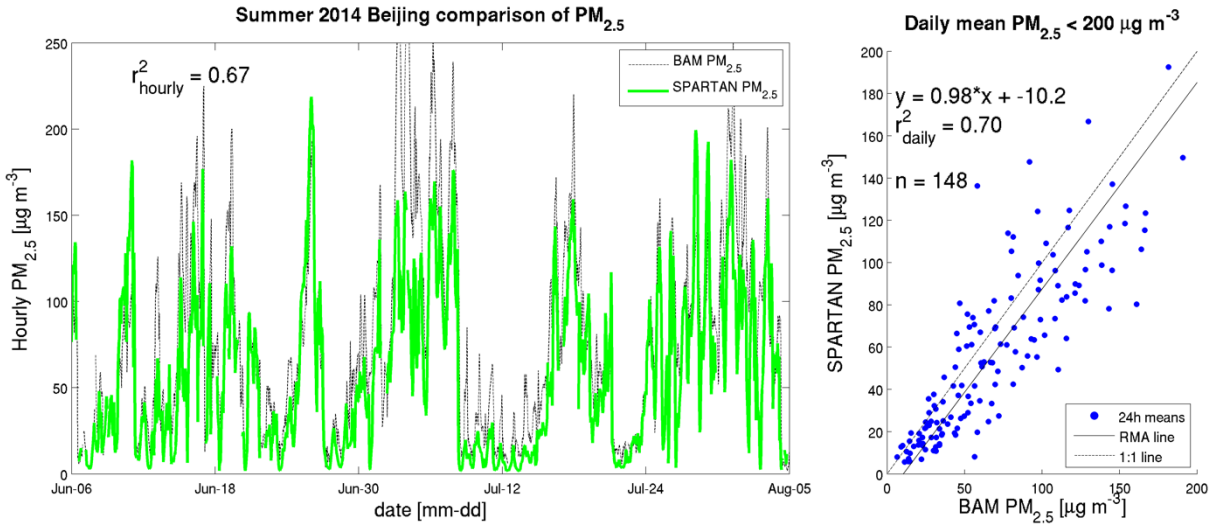| $PM_{2.5}$ mass = $\mu g\ m^{-3}$ ($1\sigma/\sqrt{n}$), components = % (1σ)		
This study (total mass = $\mu g\ m^{-3}$)	**Prior Study ($\mu g\ m^{-3}$)**	**Prior Study ($\mu g\ m^{-3}$)**
Beijing $PM_{2.5}$: 69 (3), *n* = 114 8.5 (10)% ANO_3, 19 (12)% ASO_4, 2.3 (3.3)% SS, 25 (14)% CM, 8.8 (5.3)% EBC, 37 (27)% RM	(Yang et al., 2011) 2005-2006, OM/OC = 1.7, $PM_{2.5}$: 119(40) 11 (7)% ANO_3, 17 (10)% ASO_4, 1.3 (0.6)% SS, 19 (3)% CM, 7 (5)% EC, 33 (16)% OM, 10 (10)% Unk	(Oanh et al., 2006) 2001-2004, OM/OC = 1.7 $PM_{2.5}$: 136 (45) 12 (1.5)% ANO_3, 20 (1.8)% ASO_4, 1.2 (1.2)% SS, 5 (3)% CM, 9 (7)% EBC, 29 (22)% OM, 24 (24)% Unk
Bandung $PM_{2.5}$: 31 (1), *n* = 77 2.4 (1.4)% ANO_3, 21 (8)% ASO_4, 1.0 (0.3)% SS, 8.6 (4.1)% CM, 13 (4)% EBC, 55 (19)% RM	(Oanh et al., 2006) 2001-2004. OM/OC = 2.2, $PM_{2.5}$: 45.5(10.6), 13(4)% ANO_3, 21(3)% ASO_4, 1.6(0.2)% SS, 6.6(0.5)% CM, 19 (4)% EBC, 36(11)% RM	(Lestari and Mauliadi, 2009) 2001- 2007, OM/OC = 2.2 $PM_{2.5}$: 43.5(10.5) 4(6)% ANO_3, 4(4)% ASO_4, 3(2)% SS, 23(21)% CM, 24(14)% EBC, 42(35)% RM
Manila $PM_{2.5}$: 18 (1), *n* = 63 1.8 (1.2)% ANO_3, 16 (9)% ASO_4, 2.9 (2.4)% SS, 11 (6)% CM, 25 (19)% EBC, 43 (21)% RM	(Cohen et al., 2009) 2001-2007, OM/OC = 2.1, $PM_{2.5}$: 46 (19), ANO_3 N/A 14 (9)% ASO_4, 0.6 (1.5)% SS, 5 (1.7)% CM, 25 (11)% EBC, 57(22)% OM,	
Kanpur $PM_{2.5}$: 99 (9), *n* = 33 7.4 (5.7)% ANO_3, 19 (13)% ASO_4, 0.7 (0.3)% SS, 4.8 (2.9)% CM, 9 (5.0)% EBC, 59 (35)% RM	(Behera and Sharma, 2010) Oct. 2007 – Jan 2008, OM/OC = 2.2, $PM_{2.5}$: 172 (73), 6.1 (1.3)% ANO_3, 18 (4)% ASO_4, 2.6 (0.6)% SS, 10 (3)% CM, 4.8 (1.1)% EC, 42 (9)% OM, 16 (10)% Unk	(Ram et al., 2012) Dec 2008 – Feb 2009, OM/OC = 2.2 $PM_{2.5}$: 158 (47) 6.6(4)% ANO_3, 13 (5)% ASO_4, 1.5 (0.9)% SS, 12 (6)% CM*, 3 (1.1)% EC, 57 (23)% OM, 6 (24)% Unk *Assuming CM = [Ca]/0.034 (Wang, 2015)
Mammoth Cave NP $PM_{2.5}$: 13.6 (2), *n* = 19 1.2 (1.0)% ANO_3, 33 (19)% ASO_4, 0.8 (0.8)% SS, 11 (11)% CM, 5.6 (3.2)% EBC, 49 (34)% RM	(IMPROVE, 2015) June-Aug. 2014, OM/OC = 2.0, $PM_{2.5}$: 10.0 (5.8), 2.4 (2.5)% ANO_3, 36 (17)% ASO_4, 0.3 (1.6)% SS, 7 (8)% CM, 3 (3)% EC, 34 (30)% OM, 17% Unk+H_2O	
Atlanta $PM_{2.5}$: 9.1 (1), *n* = 13 3.5 (1.2)% ANO_3, 23 (11)% ASO_4, 1.2 (1.2)% SS, 12 (4.7)% CM, 11 (2.6)% EBC, 48 (25)% RM	(Butler et al., 2003) Mar. 1999 –2000 Feb, OM/OC = 2.0, $PM_{2.5}$: 24.2 4 (0.2)% ANO_3, 28 (1.0)% ASO_4, 10 (0.8)% CM, 3 (0.2)% EC, 55 (5)% OM,	EPA Jan-May (USEPA, 2015), OM/OC = 2.0 $PM_{2.5}$: 8.5 12 (5)% ANO_3, 23 (15)% ASO_4, 1.4 (0.6)% SS 12 (5)% CM, 9.3 (5)% EC, 43 (36)% OM,
Hanoi $PM_{2.5}$: 39 (4), *n* = 10 4.4 (1.1)% ANO_3, 17 (6)% ASO_4, 2.5 (0.6)% SS, 16 (15)% CM, 10 (5.8)% EBC, 51 (22)% RM	(Cohen et al., 2010). 2001 –2008 OM/OC = 2.1, $PM_{2.5}$: 54 (33) ANO_3 N/A 29 (20)% ASO_4, 0.6 (1.4)% SS 13 (7)% CM, 8 (3)% EBC, 40 (19)% OM, 2 (2)% Unk + ANO_3	

Figure 4: Left Hourly PM$_{2.5}$ estimated from SPARTAN overlaid with a MetOne BAM-1020 (June-August 2014) at the Beijing US Embassy (15 km away). Right: 24-hour SPARTAN PM$_{2.5}$ compared with BAM for the year 2014. Reduced major axis (RMA) slope and Pearson correlations for PM$_{2.5}$ are given in inset.

Appendix:

Appendix A1:

Table A1: Hygroscopicity parameter κ_v for various studies on organic material

κ_v (OM)	Comments	Reference
0.045	Fitted to an aged organic mixture, subsaturated	(Varutbangkul et al., 2006)
0	IMPROVE network, subsaturated	(Hand and Malm, 2006)
0.10 ± 0.04	RH > 99%, fitted to SOA precursors	(Prenni et al., 2007)
$\mathbf{-0.067 + 0.33}$(O:C)	Fitted, RH > 99%	(Jimenez et al., 2009)
$\mathbf{0.29}$(O:C)	RH > 99%, 0.3 < O:C < 0.6	(Chang et al., 2010)
0.05	Best estimate from aged mixtures, subsaturated	(Dusek et al., 2011)
0.01 – 0.2	Field studies & smog chamber, subsaturated	(Duplissy et al., 2011)
0.16	RH > 99%	(Asa-Awuku et al., 2011)
0.05 – 0.13	Lab experiments, aged with H_2O_2 and light; subsaturated	(Liu et al., 2012)
0.1	RH > 99%, D_{dry} < 100 nm	(Padró et al., 2012)
$\mathbf{0.12\varepsilon_{WSOM}}$[#]	RH > 99%	(Lathem et al., 2013)
$\mathbf{-0.005 + 0.19}$(O:C)	Fitted, RH > 99% 100 nm particles	(Rickards et al., 2013)
0.03, 0.1	HDTMA-measure, subsaturated	(Bezantakos et al., 2013)
0.1	Subsaturated	Selected for this study

[#]ε_{WSOM} = fraction of water-soluble organic material.

Appendix A2:

Dry aerosol scatter ($b_{sp,\text{dry}}$) is related to relative humidity (RH) by

$$b_{sp,\text{dry}} = \frac{b_{sp}(\text{RH})}{f_v(\text{RH})} \qquad \text{Eq. A1}$$

Changes in scatter are also proportional to mass (Chow et al., 2006; Wang et al., 2010)

$$b_{sp,\text{dry}} = \alpha \text{PM}_{2.5,\text{dry}} \qquad \text{Eq. A2}$$

where α (m^2 g^{-1}) is the mass scattering efficiency and a function of aerosol size distribution, effective radius, and dry composition. In this study we treat composition, density, and size distribution as constant over each of our 9-day intermittent sampling periods so that $\alpha \approx \langle \alpha \rangle_{9d}$. Under this assumption the predicted mass changes in low humidity (35% RH) are proportional to water-free aerosol scatter:

$$\text{PM}_{2.5,\text{dry}} = \langle \text{PM}_{2.5,\text{dry}} \rangle \frac{b_{sp,\text{dry}}}{\langle b_{sp,\text{dry}} \rangle} \qquad \text{Eq. A3}$$

where $<>$ indicates 9-day averages. The explicit compensation for aerosol water is then

$$[\text{PM}_{2.5,\text{dry}}] = \frac{\langle [\text{PM}_{2.5,\text{dry}}] \rangle}{\langle b_{sp}(\text{RH})/f_v(\text{RH}) \rangle} \cdot \frac{b_{sp}(\text{RH})}{f_v(\text{RH})} \qquad \text{Eq. A4}$$

where [] indicates concentration in µg m^{-3}. Uncertainties are a function of replicate weighing measurements ($\pm$ 4 µg), flow volume ($\pm$ 10%), %RH ($\pm$ 2.5), aerosol scatter ($\pm$ 5%), and κ_v ($\pm$ 0.05).

$$\left(\frac{\delta[\text{PM}_{2.5,\text{h}}]}{[\text{PM}_{2.5,\text{h}}]} \right)^2 \approx \left(\frac{\delta \text{PM}_{2.5}}{\text{PM}_{2.5}} \right)^2 + \left(\frac{\delta V}{V} \right)^2 + \left(\frac{\delta b_{sp}}{b_{sp}} \right)^2 + \left(\frac{\delta f_v}{f_v} \right)^2 \qquad \text{Eq. A5}$$

where

$$\left(\frac{\delta f_v}{f_v} \right)^2 = \frac{(f_v - 1)^2}{f_v^2} \left[\left(\frac{\delta \kappa}{\kappa} \right)^2 + \left(\frac{\delta \text{RH}}{\text{RH} \cdot (100 - \text{RH})} \right)^2 \right] \qquad \text{Eq. A6}$$

The average relative 2-σ PM$_{2.5}$ uncertainty was 26% for dry hourly predictions, increasing with higher RH cutoffs. A cut-off of RH = 80% has been applied to our data, above which hygroscopic uncertainties, as well as total water mass, dominate.